



Dedicated to innovation in aerospace

NLR-TP-2016-025 | February 2016

A Flight Dynamics Model for a Small-Scale Flybarless Helicopter

CUSTOMER: Netherlands Aerospace Centre



NLR – Netherlands Aerospace Centre

Netherlands Aerospace Centre

NLR is a leading international research centre for aerospace. Bolstered by its multidisciplinary expertise and unrivalled research facilities, NLR provides innovative and integral solutions for the complex challenges in the aerospace sector.

NLR's activities span the full spectrum of Research Development Test & Evaluation (RDT & E). Given NLR's specialist knowledge and facilities, companies turn to NLR for validation, verification, qualification, simulation and evaluation. NLR thereby bridges the gap between research and practical applications, while working for both government and industry at home and abroad. NLR stands for practical and innovative solutions, technical expertise and a long-term design vision. This allows NLR's cutting edge technology to find its way into successful aerospace programs of OEMs, including Airbus, Embraer and Pilatus. NLR contributes to (military) programs, such as ESA's IXV re-entry vehicle, the F-35, the Apache helicopter, and European programs, including SESAR and Clean Sky 2. Founded in 1919, and employing some 650 people, NLR achieved a turnover of 73 million euros in 2014, of which three-quarters derived from contract research, and the remaining from government funds.

For more information visit: www.nlr.nl

A Flight Dynamics Model for a Small-Scale Flybarless Helicopter



Problem area

There has been considerable worldwide activity in research related to modeling and control of small-scale helicopter Unmanned Aerial Vehicles (UAVs). For low to high control input bandwidth, demonstration (or simulation) of automatic helicopter flight has been reported in numerous publications. However, none of the model-based published results are applicable for steep descent flight conditions, such as in the Vortex-Ring-State (VRS) or autorotation (helicopter flight with engine OFF).

REPORT NUMBER

NLR-TP-2016-025

AUTHOR(S)

S. Taamallah

REPORT CLASSIFICATION

UNCLASSIFIED

DATE

February 2016

KNOWLEDGE AREA(S)

Helikoptertechnologie
Computational Mechanics
and Simulation Technology

DESCRIPTOR(S)

Helicopter flight dynamics
Autorotation
Unmanned Aerial Vehicles

Description of work

We present a helicopter flight dynamics nonlinear model for a flybarless, articulated, Pitch-Lag-Flap (P-L-F) main rotor with rigid blades, particularly suited for small-scale UAVs. The model incorporates the main rotor, tail rotor, fuselage, and tails. This model is further applicable for high bandwidth control specifications, and is valid for a range of flight conditions, including the VRS and autorotation. Additionally, the paper reviews all assumptions made in deriving the model, i.e. structural, aerodynamics, and dynamical simplifications. Simulation results show that this nonlinear model is in good agreement with an equivalent FLIGHTLAB model, for both static (trim) and dynamic conditions.

Results and conclusions

The first building-block—towards the development of an autonomous helicopter system—is presented, and can be characterized as a comprehensive modeling framework, particularly suited for small-scale flybarless helicopters. Comparisons with an equivalent FLIGHTLAB simulation shows that our model is valid for a range of flight conditions, including steep descent flights and autorotation.

Applicability

This model could potentially be used for several applications: 1) simulation of the flight dynamics of small-scale (articulated or hingeless) flybarless helicopters; 2) investigation of the coupling between flap/lag and inflow dynamics; as well as 3) providing a basis for model-based control design.

GENERAL NOTE

This report is based on a paper published in the ASME Journal of Dynamic Systems, Measurement, and Control, 138(1), 2016.

NLR

Anthony Fokkerweg 2
1059 CM Amsterdam

p) +31 88 511 3113 f) +31 88 511 3210

e) info@nlr.nl i) www.nlr.nl



Dedicated to innovation in aerospace

NLR-TP-2016-025 | February 2016

A Flight Dynamics Model for a Small-Scale Flybarless Helicopter

CUSTOMER: Netherlands Aerospace Centre

AUTHOR(S):


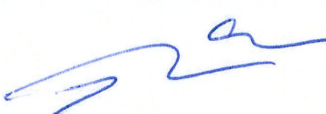

S. Taamallah

Netherlands Aerospace Centre

This report is based on a paper published in the ASME Journal of Dynamic Systems, Measurement, and Control, 138(1), 2016.

The contents of this report may be cited on condition that full credit is given to NLR and the author(s).

CUSTOMER	Netherlands Aerospace Centre
CONTRACT NUMBER	----
OWNER	Netherlands Aerospace Centre
DIVISION NLR	Aerospace Systems
DISTRIBUTION	Unlimited
CLASSIFICATION OF TITLE	UNCLASSIFIED

APPROVED BY :		
AUTHOR	REVIEWER	MANAGING DEPARTMENT
S. Taamallah 		
DATE 1 5 0 2 1 6	DATE 1 5 0 2 1 6	DATE 1 5 0 2 1 6

Contents

Abstract	5
Nomenclature	5
1 Introduction	7
1.1 Main Contribution	8
2 Rigid Body Equations of Motion	8
2.1 Assumptions	8
2.2 Modeling	8
3 Main Rotor	10
3.1 Assumptions	10
3.2 Comments on the modeling assumptions and model simplifications	11
3.3 Position and Velocity of a Blade Element	12
3.4 Flap-Lag Equations of Motion	15
3.4.1 Flap Angle as a Fourier Series	17
3.4.2 Virtual Work and Virtual Displacements	17
3.4.3 Generalized Forces (Gravity)	18
3.4.4 Generalized Forces (Aerodynamic)	19
3.4.5 Generalized Forces (Hub Damping and Spring Restraints)	20
3.5 Rotor Inflow	20
3.6 Forces and Moments	21
3.7 Rotor RPM Dynamics	22
4 Tail Rotor	22
4.1 Assumptions	22
4.2 Forces and Moments	23
5 Fuselage	24
5.1 Assumptions	24
5.2 Forces and Moments	24
6 Vertical and Horizontal Tails	24
6.1 Assumptions	24
6.2 Forces and Moments	25
7 Simulation Results	25
7.1 Trim Results	25
7.2 Dynamic Results	32
8 Conclusion	32
References	36

This page is intentionally left blank.

A Flight Dynamics Model for a Small-Scale Flybarless Helicopter

Skander Taamallah

National Aerospace Laboratory (NLR)

Anthony Fokkerweg 2, 1059 CM, Amsterdam, The Netherlands

Email: staamall@nlr.nl

ABSTRACT

We present a helicopter flight dynamics nonlinear model for a flybarless, articulated, Pitch-Lag-Flap (P-L-F) main rotor with rigid blades, particularly suited for small-scale Unmanned Aerial Vehicles (UAVs). The model incorporates the main rotor, tail rotor, fuselage, and tails. This model is further applicable for high bandwidth control specifications, and is valid for a range of flight conditions, including the Vortex-Ring-State (VRS) and autorotation. Additionally, the paper reviews all assumptions made in deriving the model, i.e. structural, aerodynamics, and dynamical simplifications. Simulation results show that this nonlinear model is in good agreement with an equivalent FLIGHTLAB model, for both static (trim) and dynamic conditions.

Nomenclature

Frames²

- F_I Geocentric inertial frame
- F_E Normal earth fixed frame
- F_o Vehicle carried normal earth frame
- F_k Kinematic (flight path) frame
- F_b Body (vehicle) frame
- F_{HB} Hub-Body frame (see Fig. 3 and Fig. 4)
- $F_{1<i<6}, F_{bl}$ Main Rotor frames (see Fig. 3 and Fig. 4)
- A Origin of frame F_I , earth center
- G Origin of frames F_b and F_k , vehicle CG
- H Origin of frame F_{HB}
- O Origin of frames F_E and F_o an earth surface point

Angles between frames

- ψ Azimuth angle (yaw angle, heading)
- θ Inclination angle (pitch angle, or elevation)
- ϕ Bank angle (roll angle)

Linear velocities \mathbf{V} and their components u, v, w

- $\mathbf{V}_{k,G}$ Kinematic velocity of vehicle CG
- $\mathbf{V}_{a,G}$ Aerodynamic velocity of vehicle CG
- $u_k^o = V_N$ x component of $\mathbf{V}_{k,G}$ on F_o , North velocity
- $v_k^o = V_E$ y component of $\mathbf{V}_{k,G}$ on F_o , East velocity
- $w_k^o = V_Z$ z component of $\mathbf{V}_{k,G}$ on F_o , Vertical velocity
- $u_k^b = u$ x component of $\mathbf{V}_{k,G}$ on F_b
- $v_k^b = v$ y component of $\mathbf{V}_{k,G}$ on F_b
- $w_k^b = w$ z component of $\mathbf{V}_{k,G}$ on F_b
- u_w, v_w, w_w Wind velocities in F_E

²The first five frames are the standard aircraft navigation frames (see for example [1]).

Angular velocities Ω and their components p, q, r $\Omega_k = \Omega_{bE}$ Kinematic angular velocity of vehicle CG relative to the earth $p_k^b = p$ Roll velocity (roll rate) of vehicle CG wrt to the earth $q_k^b = q$ Pitch velocity (pitch rate) of vehicle CG wrt to the earth $r_k^b = r$ Yaw velocity (yaw rate) of vehicle CG wrt to the earth**Main Rotor (MR) properties** α wake angle wrt to rotor disk α_{bl} Blade section angle of attack B Tip loss factor β_{bl} Blade flap angle β_0 Rotor TPP coning angle β_{1c} Longitudinal rotor TPP tilt β_{1s} Lateral rotor TPP tilt β_P Rotor precone angle $C_0 = M_{bl} \cdot y_{G_{bl}}$ Blade 1st mass moment c_{bl} Blade chord $c_{d_{bl}}$ Blade section drag coefficient $c_{l_{bl}}$ Blade section lift coefficient c_M Blade section pitching moment due to airfoil camber e_F Distance between lag and flap hinge e_L Distance between pitch and lag hinge e_P Distance between Hub and pitch hinge $\Delta_e = e_P + e_L + e_F$ Distance between Hub and flap hinge $\eta_\beta = 1/2R_{bl}^2/(1 - (e_P + e_L + e_F))$ $\eta_\zeta = 1/2R_{bl}^2/(1 - (e_P + e_L))$ Γ MR rotation, *CCW* : $\Gamma = 1$ *CW* : $\Gamma = -1$ G_{eff} Ground effect corrective factor I_b Blade 2nd mass moment (inertia about rotor shaft) I_β Blade 2nd mass moment (inertia about flap hinge) i_s Shaft tilt-angle $K_{(\theta\beta)}$ Pitch-flap coupling ratio $K_{(\theta\zeta)}$ Pitch-lag coupling ratio K_{D_β} Hub spring damper coef. (due to flap) K_{D_ζ} Hub spring damper coef. (due to lag) K_{S_β} Hub spring restraints coef. (due to flap) K_{S_ζ} Hub spring restraints coef. (due to lag) $\lambda_0, \lambda_c, \lambda_s$ Uniform, longitudinal, lateral inflows M_{bl} Blade mass from flap hinge N_b Number of blades Ω_{MR} Instantaneous angular velocity ψ_{bl} Azimuthal angular position of blade ψ_{PA} Swashplate phase angle R_{bl} Blade radius measured from flap hinge R_{rot} Rotor radius measured from hub center r_c Blade root cutout r_{dm} Distance from flap hinge to element dm θ_{bl} Blade pitch outboard of flap hinge θ_{wash} Blade twist (or washout) at blade tip x_H, y_H, z_H Coordinates of MR Hub wrt vehicle CG in F_b V_M Mass flow parameter $V_{ref} = \Omega_{MR} \cdot R_{rot}$ Reference velocity V_T Non-dimensional total velocity at rotor center v_i Rotor induced velocity v_{i0}, v_{ic}, v_{is} Uniform, longitudinal, lateral induced velocities $y_{G_{bl}}$ Blade CG radial position from flap hinge ζ_{bl} Blade lag angle

Tail Rotor (TR) properties

B_{TR}	Tip loss factor, expressed as percentage of blade length
β_{0TR}	Tail rotor coning angle
b_{t1}	Tail blockage constant
CD_{TR}	Mean drag coefficient (profile drag)
$c_{l(0,TR)}$	Blade section lift curve slope
c_{TR}	Blade chord
δ_{3TR}	Hinge skew angle for pitch-flap coupling
λ_{dw}	Downwash
λ_{TR}	Total inflow
$\mu_{TRx}, \mu_{TRY}, \mu_{TRz}$	x-, y-, and z-component of advance ratio
N_{bTR}	Tail rotor number of blades
Ω_{TR}	Instantaneous angular velocity
R_{rotTR}	Rotor radius measured from shaft
$\sigma_{TR} = N_{bTR} \frac{c_{TR}}{\pi R_{rotTR}}$	Solidity
θ_{biasTR}	Preset collective pitch bias
x_{TR}, y_{TR}, z_{TR}	Coordinates of TR Hub wrt vehicle CG in F_b
v_{bl}	Transition velocity (vertical fin blockage)

Fuselage (Fus) properties

α_{Fus}	Angle of attack
β_{Fus}	Sideslip angle
L_{refFus}	Reference length
S_{refFus}	Reference area
$x_{Fus}, y_{Fus}, z_{Fus}$	Coordinates of Fus aero center wrt vehicle CG in F_b

Control Inputs

θ_0	MR blade root collective pitch
θ_{1c}	MR lateral cyclic pitch
θ_{1s}	MR longitudinal cyclic pitch
θ_{TR}	TR blade pitch angle

Misc.

g	Acceleration due to gravity
\mathbb{I}_V	Vehicle inertia
M	Mach number
m_V	Vehicle mass
ρ	Air density
x_N, x_E, x_Z	Coordinates of vehicle CG in F_o

Vectors are printed in boldface \mathbf{X} . A vector is qualified by its subscript, whereas its superscript denotes the projection frame: e.g. \mathbf{V}_a^I represents the aerodynamic velocity projected on frame F_I . Matrices are written in outline type \mathbb{M} , and transformation matrices are denoted as \mathbb{T}_{ij} , with the two suffices signifying from frame F_j to frame F_i . All units are in the S.I. system.

1 Introduction

Over the past thirty years, significant scientific progress related to sensors technology and computational miniaturized hardware has allowed for sustained improvements in the fields of robotics and automation, leading to major advancement in the area of flying robots, also known as Unmanned Aerial Vehicles (UAVs) [2, 3]. These unmanned vehicles have been developed for both civilian and military missions, with their *raison d'être* stemming primarily from the need for (near) real-time information. In some cases, UAV deployment and recovery from unprepared or confined sites may also be required, such as when operating from or above urban and natural canyons, forests, or from naval ships. Hence, and for those specific situations, a helicopter UAV capable of flying autonomously, in and out of such restricted areas, would represent a particularly attractive asset. There has been considerable worldwide activity in research related to modeling and control of small-scale helicopter UAVs. For low to medium control input bandwidth, demonstration (or simulation) of automatic helicopter flight, for the case of hover and low speed flight conditions, has been shown in [4–12]. On the other hand, for high bandwidth system specifications, at still these conventional flight conditions, model-based automatic flight results can be found in [13–23], and non model-based examples³ have been documented in [24–27], whereas vision based systems have been reported in [28–

³In the areas of machine learning, evolutionary, and genetic algorithms.

32]. For the case of high bandwidth system specifications, at non-conventional flight conditions (e.g. aggressive/aerobatic flights), model-based approaches have been described in [33–35], whereas non-model-based approaches have been reported in [36–38]. However, and to the best of our knowledge, none of the previous model-based results are applicable for steep descent flight conditions, such as in the Vortex-Ring-State (VRS) or autorotation (helicopter flight with engine OFF).

1.1 Main Contribution

The novel part of this paper consists in deriving the coupled flap-lag equations of motion, for a rigid, flybarless⁴, articulated rotor, with a Pitch-Lag-Flap (P-L-F) rotor hinge sequence. This represents the main contribution of the paper from a mathematical modeling viewpoint. An additional contribution consists in integrating various available modeling results from the literature (e.g. main and tail rotors inflow), in order to present a comprehensive flight dynamics model for a small-scale, flybarless helicopter UAV, applicable for high bandwidth control specifications, and valid for a range of flight conditions, including (steep) descent flight into the VRS and autorotation [39, 40]. Whereas preliminary results of our nonlinear model have been presented in [41, 42], in this paper the model includes the twelve-states rigid body equations of motion, and for each blade the four-states flap/lag angles and rotational velocities. It further includes the three-states dynamic inflow, and the single-state main rotor Revolutions Per Minute (RPM)⁵, see Fig. 1. The tail rotor has been modeled as a Bailey type rotor. The fuselage model is based upon aerodynamic lift and drag coefficients, which are tabulated as a function of airflow Angle Of Attack (AOA) and sideslip angles. The horizontal and vertical tails are based upon standard flat plate models. Finally, the paper reviews all assumptions made in deriving the model, i.e. structural, aerodynamics, and dynamical simplifications. A full version of this model has been used as a realistic small-scale helicopter simulation environment, simplified versions have been used for the generation of optimal trajectories [43–45], and linearizations of this nonlinear model have been used for the design of trajectory trackers [46].

The remainder of this paper is organized as follows. In Section 2, the rigid body equations of motion are summarized. In Section 3 and 4, main and tail rotor models are discussed. In Section 5, the fuselage model is reviewed. In Section 6, comments are made on the vertical and horizontal tail models. In Section 7, simulation results are analyzed. Finally, conclusions and future directions are presented in Section 8.

2 Rigid Body Equations of Motion

2.1 Assumptions

1. The vehicle has a longitudinal plane of symmetry, and has constant mass, inertia, and Center of Gravity (CG) position, hence fuel consumption and/or payload pickup/release are neglected. The vehicle is also a rigid system, i.e. it does not contain any flexible structures, hence the time derivative of the inertia matrix is zero.
2. The vehicle Altitude above Ground Level (AGL) is very small compared to the earth radius, implying a gravitation independent of height and thus constant.
3. The earth is assumed fixed and flat.

2.2 Modeling

Classical Newtonian mechanics and the fundamental relationship of kinematics give the standard twelve-states rigid body equations of motion (following notations of [1] and the nomenclature given at the beginning of the paper)

$$\begin{pmatrix} \dot{x}_N \\ \dot{x}_E \\ \dot{x}_Z \end{pmatrix}^o = \begin{pmatrix} V_N \\ V_E \\ V_Z \end{pmatrix}^o \quad \begin{pmatrix} V_N \\ V_E \\ V_Z \end{pmatrix}^o = \mathbb{T}_{ob.} \begin{pmatrix} u \\ v \\ w \end{pmatrix}^b \quad (1)$$

$$\begin{pmatrix} \dot{u} \\ \dot{v} \\ \dot{w} \end{pmatrix}^b = - \begin{pmatrix} q.w - r.v \\ r.u - p.w \\ p.v - q.u \end{pmatrix}^b + g \cdot \begin{pmatrix} -\sin\theta \\ \cos\theta\sin\phi \\ \cos\theta\cos\phi \end{pmatrix}^b + \frac{\mathbf{F}_{CG}}{m_V}^b \quad (2)$$

$$\begin{pmatrix} \dot{p} \\ \dot{q} \\ \dot{r} \end{pmatrix}^b = \mathbb{I}_V^{-1} \cdot \left(\mathbf{M}_{CG}^b - \begin{pmatrix} p \\ q \\ r \end{pmatrix}^b \right) \times \left(\mathbb{I}_V \cdot \begin{pmatrix} p \\ q \\ r \end{pmatrix}^b \right) \quad (3)$$

⁴Without a Bell-Hiller stabilizing bar.

⁵The RPM state is an essential part of the autorotative flight condition.



Fig. 1: Helicopter Inputs \mathbf{u} (in green), States \mathbf{x} (in blue the rigid-body states, in red the main rotor states), and Measurements \mathbf{y} (measured states)

$$\begin{pmatrix} \dot{\phi} \\ \dot{\theta} \\ \dot{\psi} \end{pmatrix}^b = \begin{bmatrix} 1 & \sin \theta \cdot \frac{\sin \phi}{\cos \theta} & \sin \theta \cdot \frac{\cos \phi}{\cos \theta} \\ 0 & \cos \phi & -\sin \phi \\ 0 & \frac{\sin \phi}{\cos \theta} & \frac{\cos \phi}{\cos \theta} \end{bmatrix} \cdot \begin{pmatrix} p \\ q \\ r \end{pmatrix}^b \quad (4)$$

$$\text{with } \mathbb{T}_{ob} = \begin{bmatrix} \cos \theta \cos \psi & (\sin \theta \sin \phi \cos \psi - \sin \psi \cos \phi) & (\cos \psi \sin \theta \cos \phi + \sin \phi \sin \psi) \\ \sin \psi \cos \theta & (\sin \theta \sin \phi \sin \psi + \cos \psi \cos \phi) & (\sin \theta \cos \phi \sin \psi - \sin \phi \cos \psi) \\ -\sin \theta & \cos \theta \sin \phi & \cos \theta \cos \phi \end{bmatrix} \quad (5)$$

and \mathbf{F}_{CG}^b all external forces, excluding gravity, experienced by the vehicle CG in the body frame F_b , and \mathbf{M}_{CG}^b the moments of all forces expressed at the vehicle CG in frame F_b . These total forces and moments include contributions from the Main Rotor (MR), Tail Rotor (TR), Fuselage (Fus), Vertical Tail (VT), and Horizontal Tail (HT), and are given by

$$\begin{aligned} \mathbf{F}_{CG}^b &= \mathbf{F}_{MR}^b + \mathbf{F}_{TR}^b + \mathbf{F}_{Fus}^b + \mathbf{F}_{VT}^b + \mathbf{F}_{HT}^b \\ \mathbf{M}_{CG}^b &= \mathbf{M}_{MR}^b + \mathbf{M}_{TR}^b + \mathbf{M}_{Fus}^b + \mathbf{M}_{VT}^b + \mathbf{M}_{HT}^b \end{aligned} \quad (6)$$

3 Main Rotor

For a single main rotor, and briefly summarized, helicopter flight dynamics includes the rigid-body responses (presented in the previous section) combined with the main rotor higher-frequency modes [47, 48]. For flight mechanics and control development purposes, the three most important aspects of these higher-order rotor modes are: 1) blade flapping, which allows the blade to move in a plane containing the blade and the shaft; 2) blade lead-lag, which allows the blade to move in the plane of rotation; and 3) rotor inflow which is the flow field induced by the main rotor. Now, for the case of a fully articulated rotor system, each rotor blade is attached to the rotor hub through a series of hinges, which allow each blade to move independently of the others. However, for small-scale helicopters, the rotor hub generally includes a pitch (feathering) hinge close to the shaft, and a lead-lag hinge⁶ further outboard. Besides the hub is typically not equipped with a flap hinge, this latter is often replaced by stiff rubber rings, hence a so-called hingeless flap mechanism, see Fig. 2. But for the purpose of helicopter flight dynamics modeling, it is standard practice to model a hingeless rotor (and its flexible blades) as a rotor having rigid blades attached to a virtual hinge [49], this latter being offset from the main rotor axis. This virtual hinge is often modeled as a torsional spring, implying stiffness and damping⁷.

In order to simulate a generic flybarless small-scale helicopter main rotor, we have chosen to model it as an articulated Pitch-Lag-Flap (P-L-F) hinge arrangement. This chosen hinge configuration is particularly well suited for the case of small-scale helicopters. Indeed, it allows to keep the pitch and lag hinge offsets at their current physical values while replacing the rubber O-rings, see Fig. 2, by a virtual flap hinge (having stiffness and damping) outboard⁸ of the lag hinge.

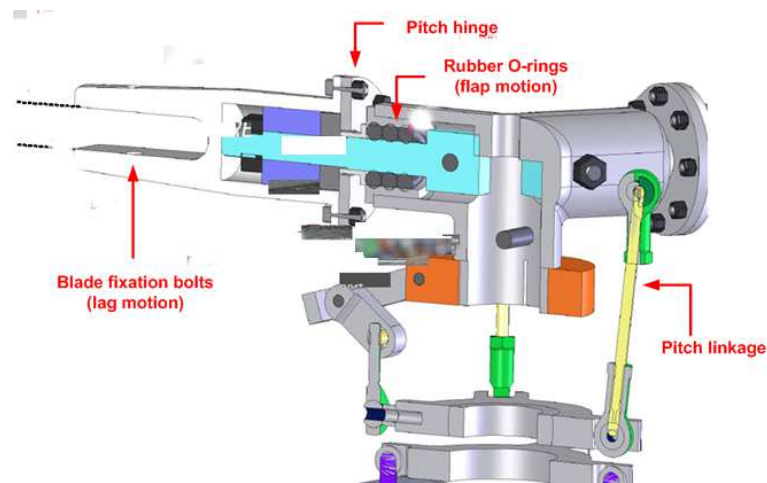


Fig. 2: NLR's Facility for Unmanned Rotorcraft REsearch (FUORE) project. Typical main rotor hub for a (small-scale) UAV helicopter (courtesy of NLR)

3.1 Assumptions

The presented assumptions are valid for stability and control investigations of helicopters up to an advance ratio limit of about⁹ 0.3 [51–53].

Structural Simplifications

1. Rotor shaft forward and lateral tilt-angles are zero. Rotor precone is also zero. The blade has zero twist, constant chord, zero sweep, constant thickness ratio, and a uniform mass distribution.
2. We assume a rigid rotor blade in bending. We neglect higher modes (harmonics), since higher modes are only pronounced at high speed [49, 54]. Further, blade torsion is neglected since small-scale helicopter blades are generally relatively stiff.
3. Rotor inertia inboard of the flap hinge is also neglected.

⁶On small-scale helicopters this is technically not a hinge, rather we refer here to the blade fixation bolt.

⁷Adjusting the virtual hinge offset distance, stiffness, and damping, allows to recreate the correct blade motion in terms of amplitude and frequency [50].

⁸Between the lag hinge and the blade tip.

⁹The flight envelope of small-scale helicopters is well within this limit.

Aerodynamics Simplifications

1. Uniform inflow is computed through momentum theory.
2. Vehicle flies at a low altitude, hence neglecting air density and temperature variations. Blade Element (BE) theory is used to compute rotor lift and drag forces. Radial flow along blade span is ignored. Pitch, lag, and flap angles are assumed to be small.
3. Compressibility effects are disregarded, which is a reasonable assumption considering small-scale helicopter flight characteristics. Viscous flow effects are also disregarded, which is a valid assumption for low AOA and un-separated flow [55,56].
4. Aerodynamic interference effects between the main rotor and other helicopter modules, e.g. fuselage or tail rotor, are neglected.
5. The presence of the fuselage just under the main rotor acts as a so-called pseudo-ground effect [57], resulting in some thrust recovery. This phenomenon is also neglected.

Dynamical Simplifications

1. Dynamic twist¹⁰ is neglected. Hence blade CG is assumed to be collocated with blade section quarter chord line.
2. Unsteady (frequency dependent) effect for time-dependent development of blade lift and pitching moment, due to changes in local incidence, are ignored; e.g. dynamic stall, due to rapid pitch changes, is ignored.
3. A balanced rotor is assumed. In general most of the inertial terms, contributing to main rotor moments, vanish when integrated around 2π azimuth.

3.2 Comments on the modeling assumptions and model simplifications

Helicopter simulation codes may be developed for a variety of applications, ranging from flight dynamics simulation purposes, flying qualities investigations, auto-pilot design, operational analysis, crew training, load prediction, and/or vibrations analysis. In our case, the desired objectives (i.e. the application domain) for our model are: 1) flight dynamics simulation, in which the model can be used in a Hardware In The loop (HITL) environment to simulate the helicopter dynamics, hence enabling the verification and validation of a flight control system (i.e. the embedded system); and 2) the model should also be useful for controller synthesis, i.e. the so-called modeling for control paradigm. This sets the context of the model presented in this paper.

Now once the intended model's application domain has been defined, we need to address the question of helicopter model fidelity. To this end, and according to [58], the level of model sophistication, to conveniently describe a helicopter model complexity, may be formulated by two criteria, namely **model dynamics** and **model validity**, defined as follows:

1. **Model dynamics** qualifies the level of detail in representing the dynamics of the helicopter. This criterium determines the fidelity of the model in terms of the frequency range of applicability, e.g. a model consisting of only the rigid-body, actuators, and main rotor RPM dynamics, versus a model which also includes additional main rotor higher-frequency phenomena, such as blade flap-lag, rotor inflow dynamics, etc.
2. **Model validity** represents the level of sophistication in calculating the helicopter forces, moments, and main rotor inflow. This criterium determines the domain of validity in the flight envelope, e.g. a model which crudely reproduces the associated laws of physics, versus a model which accurately simulates the vehicle (aerodynamic) forces and moments, including at high speed flight, descending in the Vortex-Ring-State (VRS), and the autorotation condition.

In terms of **model dynamics**, our model includes some of the main rotor higher-order phenomena, such as blade flap-lag dynamics and main rotor inflow dynamics. Hence, for its intended application domain, our model may be considered to be of good quality. This said, and as mentioned here-above in the assumptions, the dynamical aspects related to blade torsion, dynamic twist, and dynamic stall have been neglected. Thus, our model may not be valid in the very high-frequency region, i.e. it probably can not be used for a detailed analysis of vibrations and/or aeroelastic phenomena. However, as mentioned earlier, these latter aspects do not belong to the intended application domain of the proposed model.

In terms of **model validity**, the effects of compressibility and viscous flows have been disregarded, since relatively negligible on small-scale helicopters¹¹. On the other hand, our model does include a sophisticated main rotor inflow model, valid also for high-speed descent and VRS flight, but does not include any aerodynamic interference effects between the main rotor and other helicopter components, although this aspect is generally a minor one on small-scale vehicles. In summary we conclude that our model may also have a relatively high model validity for its intended application domain.

¹⁰Any offset in blade chordwise CG and/or blade aerodynamic center position will result in a coupling of the flap and torsion Degrees Of Freedom (DOF) in blade elastic modes [49].

¹¹The blade tip Mach number is below 0.4.

3.3 Position and Velocity of a Blade Element

With reference to the nomenclature for the frame's origin A , G , and H , the inertial position of a blade element dm , located at position P_{dm} , see Fig. 3 and Fig. 4, is given by

$$\mathbf{AP}_{dm} = \mathbf{AG} + \mathbf{GH} + \mathbf{HP}_{dm} \quad (7)$$

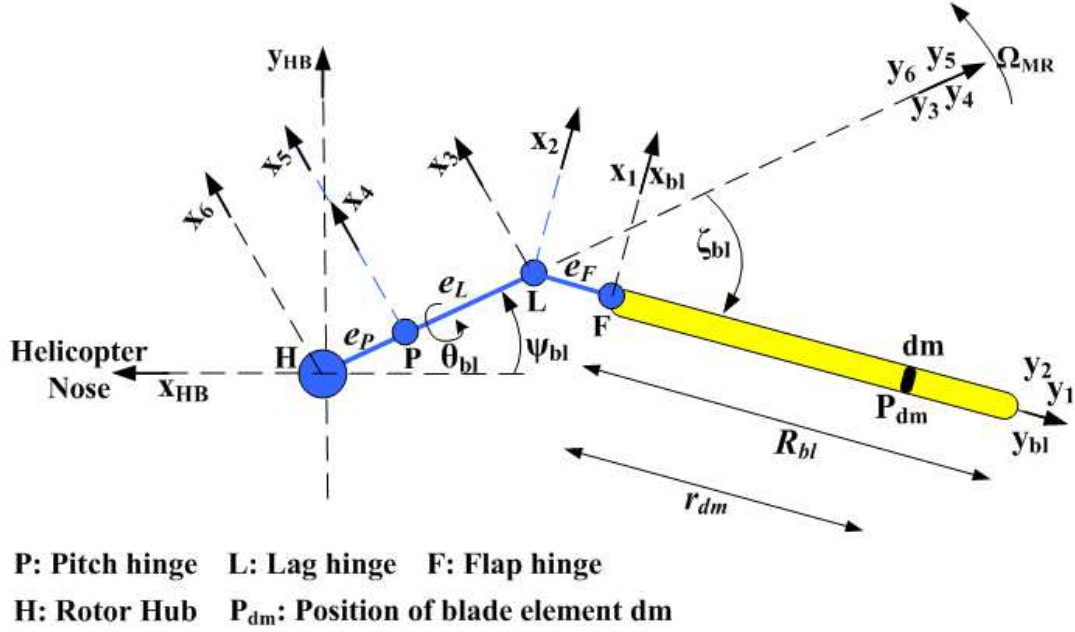


Fig. 3: Main rotor frames (top-view)

Projecting Eqn. (7) onto the Hub-Body frame F_{HB} we get

$$\mathbf{AP}_{dm}^{HB} = \mathbf{AG}^{HB} + \begin{pmatrix} x_H \\ y_H \\ z_H \end{pmatrix}^{HB} + \begin{pmatrix} x_{dm} \\ y_{dm} \\ z_{dm} \end{pmatrix}^{HB} \quad (8)$$

with (x_{dm}, y_{dm}, z_{dm}) the position of blade element dm wrt the main rotor hub. Now the third term on the Right-Hand-Side (RHS) of Eqn. (8) is given by (see Fig. 3 and Fig. 4)

$$\mathbf{HP}_{dm}^{HB} = \mathbb{T}_{(HB)6} \left\{ \mathbb{T}_{54} \left[\mathbb{T}_{32} \left(\mathbb{T}_{1(bl)} \begin{pmatrix} 0 \\ r_{dm} \\ 0 \end{pmatrix} + \begin{pmatrix} 0 \\ e_F \\ 0 \end{pmatrix} \right) + \begin{pmatrix} 0 \\ e_L \\ 0 \end{pmatrix} \right] + \begin{pmatrix} 0 \\ e_P \\ 0 \end{pmatrix} \right\} \quad (9)$$

with \mathbb{T}_{ij} rotation matrices¹². The inertial velocity, i.e. relative to the inertial frame F_I , of a blade element dm , located at position P_{dm} , is defined by $\mathbf{V}_{I,P_{dm}}$. Projecting it onto frame F_{HB} , and using Eqn. (7), we obtain

$$\mathbf{V}_{I,P_{dm}}^{HB} = \left(\frac{d\mathbf{AG}^I}{dt} \right)^{HB} + \left(\frac{d\mathbf{GH}^I}{dt} \right)^{HB} + \left(\frac{d\mathbf{HP}_{dm}^I}{dt} \right)^{HB} \quad (10)$$

¹²For example $\mathbb{T}_{(HB)6}$ represents the rotation from frame F_6 to the Hub-Body frame F_{HB} , \mathbb{T}_{54} represents the rotation from frame F_4 to frame F_5 , and $\mathbb{T}_{1(bl)}$ the rotation from the blade frame F_{bl} to frame F_1 , etc.

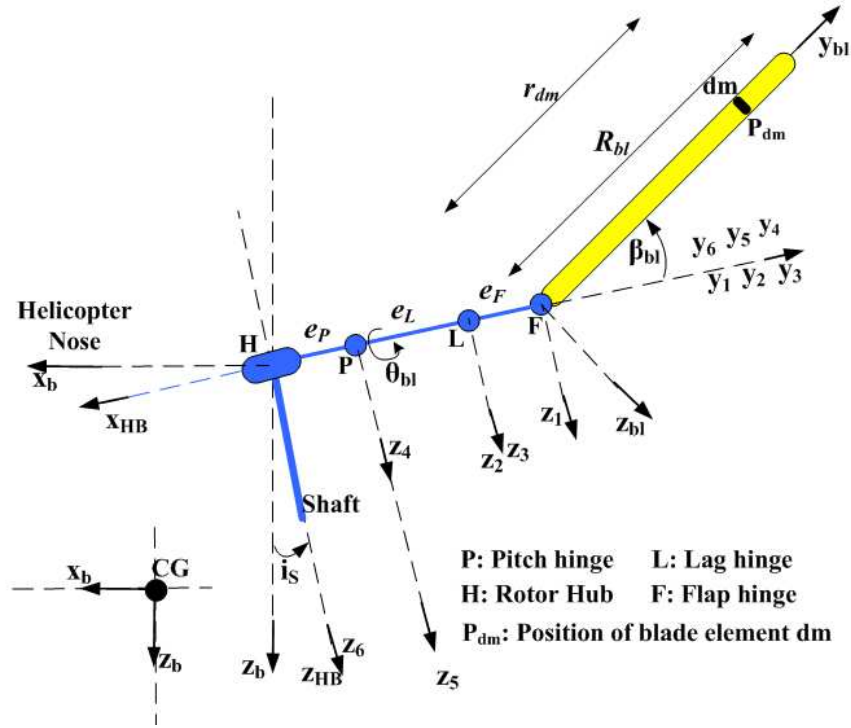


Fig. 4: Main rotor frames (side-view)

where the superscript $(\cdot)^I$, such as in $\frac{d\mathbf{AG}^I}{dt}$, means that the derivative is taken relative to inertial frame F_I . For the first term on the RHS of Eqn. (10), and assuming a flat and fixed earth, we get (refer also to the nomenclature)

$$\left(\frac{d\mathbf{AG}^I}{dt}\right)^{HB} = \mathbb{T}_{(HB)o} \mathbf{V}_{k,G}^o = \mathbb{T}_{(HB)o} \begin{pmatrix} V_N \\ V_E \\ V_Z \end{pmatrix}^o \quad (11)$$

with $\mathbf{V}_{k,G}^o$ the vehicle kinematic velocity projected onto the vehicle carried normal earth frame F_o , and $\mathbb{T}_{(HB)o}$ the rotation matrix from frame F_o to frame F_{HB} . For the second term on the RHS of Eqn. (10) we obtain (using the kinematics rule)

$$\left(\frac{d\mathbf{GH}^I}{dt}\right)^{HB} = \left(\frac{d\mathbf{GH}^b}{dt}\right)^{HB} + \boldsymbol{\Omega}_{bl}^{HB} \times \mathbf{GH}^{HB} \quad (12)$$

where \times denotes the cross product, and $\boldsymbol{\Omega}_{bl}^{HB}$ the angular velocity of body frame F_b relative to inertial frame F_I , projected onto the Hub-Body frame F_{HB} . Here the first term on the RHS of Eqn. (12) is zero since the hub center H is fixed in the body frame F_b . The second term on the RHS of Eqn. (12) gives

$$\boldsymbol{\Omega}_{bl}^{HB} \times \mathbf{GH}^{HB} = \left(\mathbb{T}_{(HB)b} \boldsymbol{\Omega}_{bl}^b\right) \times \left(\mathbb{T}_{(HB)b} \mathbf{GH}^b\right) \quad (13)$$

Since the earth is fixed we have $\boldsymbol{\Omega}_{bl}^b = \boldsymbol{\Omega}_{bE}^b$ (see nomenclature), and Eqn. (12) is now equivalent to

$$\left(\frac{d\mathbf{GH}^I}{dt}\right)^{HB} = \left(\mathbb{T}_{(HB)b} \begin{pmatrix} p \\ q \\ r \end{pmatrix}^b\right) \times \left(\mathbb{T}_{(HB)b} \begin{pmatrix} x_H \\ y_H \\ z_H \end{pmatrix}^b\right) \quad (14)$$

Finally, for the third term on the RHS of Eqn. (10) we have

$$\left(\frac{d\mathbf{HP}_{dm}^I}{dt}\right)^{HB} = \left(\frac{d\mathbf{HP}_{dm}^{HB}}{dt}\right)^{HB} + \mathbf{\Omega}_{(HB)I}^{HB} \times \mathbf{HP}_{dm}^{HB} = \frac{d}{dt} \begin{pmatrix} x_{dm} \\ y_{dm} \\ z_{dm} \end{pmatrix}^{HB} + \mathbf{\Omega}_{(HB)I}^{HB} \times \begin{pmatrix} x_{dm} \\ y_{dm} \\ z_{dm} \end{pmatrix}^{HB} \quad (15)$$

We can also express $\mathbf{\Omega}_{(HB)I}^{HB}$ as

$$\mathbf{\Omega}_{(HB)I}^{HB} = \mathbf{\Omega}_{(HB)b}^{HB} + \mathbf{\Omega}_{bI}^{HB} \quad (16)$$

The first term on the RHS of Eqn. (16) is zero since frame F_{HB} is fixed wrt frame F_b . The second term on the RHS of Eqn. (16) can be re-written as

$$\mathbf{\Omega}_{bI}^{HB} = \mathbb{T}_{(HB)b} \mathbf{\Omega}_{bI}^b = \mathbf{\Omega}_{bI}^b = \mathbf{\Omega}_{bE}^b = \begin{pmatrix} p \\ q \\ r \end{pmatrix}^b \quad (17)$$

where we have used $\mathbb{T}_{(HB)b} = \mathbb{I}$ since rotor shaft longitudinal and lateral tilt-angles i_S are assumed to be zero on our helicopter UAV. Regrouping terms from Eqn. (11), Eqn. (14), Eqn. (15), Eqn. (16), and Eqn. (17), we can express the inertial velocity of a blade element dm in F_{HB} as

$$\mathbf{V}_{I,P_{dm}}^{HB} = \begin{pmatrix} u_{I,P_{dm}} \\ v_{I,P_{dm}} \\ w_{I,P_{dm}} \end{pmatrix}^{HB} = \begin{pmatrix} u \\ v \\ w \end{pmatrix}^b + \frac{d}{dt} \begin{pmatrix} x_{dm} \\ y_{dm} \\ z_{dm} \end{pmatrix}^{HB} + \begin{pmatrix} p \\ q \\ r \end{pmatrix}^b \times \left(\begin{pmatrix} x_H \\ y_H \\ z_H \end{pmatrix}^b + \begin{pmatrix} x_{dm} \\ y_{dm} \\ z_{dm} \end{pmatrix}^{HB} \right) \quad (18)$$

where we have used

$$\mathbb{T}_{(HB)o} \begin{pmatrix} V_N \\ V_E \\ V_Z \end{pmatrix}^o = \mathbb{T}_{(HB)b} \cdot \mathbb{T}_{bo} \begin{pmatrix} V_N \\ V_E \\ V_Z \end{pmatrix}^o \quad (19)$$

together with $\mathbb{T}_{(HB)b} = \mathbb{I}$, and $\mathbb{T}_{bo} \begin{pmatrix} V_N \\ V_E \\ V_Z \end{pmatrix}^o = \begin{pmatrix} u \\ v \\ w \end{pmatrix}^b$ from the nomenclature. Now plugging Eqn. (9) into Eqn. (18), we can obtain an expanded expression for $\mathbf{V}_{I,P_{dm}}^{HB}$.

$$\begin{aligned} u_{I,P_{dm}}^{HB} = & u + \Omega_{MR} \left(\sin \psi_{bl} [e_L + e_P + \cos \zeta_{bl} (e_F + r_{dm} \cos \beta_{bl})] - \cos \psi_{bl} [\cos \theta_{bl} \sin \zeta_{bl} (e_F + r_{dm} \cos \beta_{bl}) + r_{dm} \sin \beta_{bl} \sin \theta_{bl}] \right) \\ & + \dot{\zeta}_{bl} (e_F + r_{dm} \cos \beta_{bl}) [\cos \psi_{bl} \sin \zeta_{bl} - \sin \psi_{bl} \cos \theta_{bl} \cos \zeta_{bl}] \\ & + \beta_{bl} r_{dm} [\cos \psi_{bl} \cos \zeta_{bl} \sin \beta_{bl} + \sin \psi_{bl} (\cos \theta_{bl} \sin \zeta_{bl} \sin \beta_{bl} - \cos \beta_{bl} \sin \theta_{bl})] \\ & + \dot{\theta}_{bl} \sin \psi_{bl} [\sin \theta_{bl} \sin \zeta_{bl} (e_F + r_{dm} \cos \beta_{bl}) - r_{dm} \sin \beta_{bl} \cos \theta_{bl}] + q \left(z_H - r_{dm} \cos \theta_{bl} \sin \beta_{bl} + (e_F + r_{dm} \cos \beta_{bl}) \sin \zeta_{bl} \sin \theta_{bl} \right) \\ & - r \left(y_H - \Gamma \cos \psi_{bl} (\cos \theta_{bl} \sin \zeta_{bl} (e_F + r_{dm} \cos \beta_{bl}) + r_{dm} \sin \beta_{bl} \sin \theta_{bl}) + \Gamma \sin \psi_{bl} (e_L + e_P + \cos \zeta_{bl} (e_F + r_{dm} \cos \beta_{bl})) \right) \end{aligned} \quad (20)$$

$$\begin{aligned} v_{I,P_{dm}}^{HB} = & v + \Omega_{MR} \Gamma \left((e_L + e_P) \cos \psi_{bl} + r_{dm} \sin \psi_{bl} \sin \beta_{bl} \sin \theta_{bl} + (e_F + r_{dm} \cos \beta_{bl}) (\cos \psi_{bl} \cos \zeta_{bl} + \sin \psi_{bl} \cos \theta_{bl} \sin \zeta_{bl}) \right) \\ & - \dot{\zeta}_{bl} \Gamma (e_F + r_{dm} \cos \beta_{bl}) [\cos \psi_{bl} \cos \zeta_{bl} \cos \theta_{bl} + \sin \psi_{bl} \sin \zeta_{bl}] \\ & + \beta_{bl} r_{dm} \Gamma (\cos \psi_{bl} \cos \theta_{bl} \sin \zeta_{bl} \sin \beta_{bl} - \cos \psi_{bl} \cos \beta_{bl} \sin \theta_{bl} - \sin \psi_{bl} \cos \zeta_{bl} \sin \beta_{bl}) \\ & + \dot{\theta}_{bl} \Gamma \cos \psi_{bl} [\sin \theta_{bl} \sin \zeta_{bl} (e_F + r_{dm} \cos \beta_{bl}) - r_{dm} \sin \beta_{bl} \cos \theta_{bl}] - p \left(z_H - \left(r_{dm} \cos \theta_{bl} \sin \beta_{bl} - (e_F + r_{dm} \cos \beta_{bl}) \sin \zeta_{bl} \sin \theta_{bl} \right) \right) \\ & + r \left(x_H - \left(\cos \psi_{bl} (e_L + e_P + \cos \zeta_{bl} (e_F + r_{dm} \cos \beta_{bl})) + \sin \psi_{bl} (\cos \theta_{bl} \sin \zeta_{bl} (e_F + r_{dm} \cos \beta_{bl}) + r_{dm} \sin \beta_{bl} \sin \theta_{bl}) \right) \right) \end{aligned} \quad (21)$$

$$\begin{aligned}
w_{I,P_{dm}}^{HB} &= w + \dot{\zeta}_{bl} \cos \zeta_{bl} \sin \theta_{bl} (e_F + r_{dm} \cos \beta_{bl}) - \dot{\beta}_{bl} r_{dm} (\cos \beta_{bl} \cos \theta_{bl} + \sin \beta_{bl} \sin \zeta_{bl} \sin \theta_{bl}) \\
&+ \dot{\theta}_{bl} [r_{dm} \sin \theta_{bl} \sin \beta_{bl} + (e_F + r_{dm} \cos \beta_{bl}) \sin \zeta_{bl} \cos \theta_{bl}] \\
&+ p \left(y_H - \Gamma \cos \psi_{bl} (\cos \theta_{bl} \sin \zeta_{bl} (e_F + r_{dm} \cos \beta_{bl}) + r_{dm} \sin \beta_{bl} \sin \theta_{bl}) + \Gamma \sin \psi_{bl} (e_L + e_P + \cos \zeta_{bl} (e_F + r_{dm} \cos \beta_{bl})) \right) \\
&- q \left(x_H - \cos \psi_{bl} (e_L + e_P + \cos \zeta_{bl} (e_F + r_{dm} \cos \beta_{bl})) - \sin \psi_{bl} (\cos \theta_{bl} \sin \zeta_{bl} (e_F + r_{dm} \cos \beta_{bl}) + r_{dm} \sin \beta_{bl} \sin \theta_{bl}) \right)
\end{aligned} \quad (22)$$

with the total blade pitch angle given by [59]

$$\theta_{bl} = \theta_0 + \theta_{1c} \cos(\psi_{bl} + \psi_{PA}) + \theta_{1s} \sin(\psi_{bl} + \psi_{PA}) + \theta_{t,r_{dm}} - K_{(\theta_{bl}\beta_{bl})} \beta_{bl} - K_{(\theta_{bl}\zeta_{bl})} \zeta_{bl} \quad (23)$$

and the blade pitch component due to blade twist given by

$$\theta_{t,r_{dm}} = r_{dm} \frac{\theta_{wash}}{R_{bl}} \quad (24)$$

Note also, as stated in Section 3.1, we neglect any effects due to rapid pitch changes, e.g. dynamic stall effects. Hence, in the sequel we will assume that $\theta_{bl} \ll \beta_{bl}$, $\theta_{bl} \ll \zeta_{bl}$, and $\dot{\theta}_{bl} \ll \Omega_{MR}$. Consequently, in the sequel we will also assume to have $\dot{\theta}_{bl} \approx 0$ in Eqn. (20)–Eqn. (22).

3.4 Flap-Lag Equations of Motion

Since the early 1950s it is known that including flapping dynamics in a helicopter flight model could produce limitations in rate and attitude feedback gains [60]. Further, for helicopter directional axis control, blade lead-lag dynamics ought to be considered for control system design [61]. Indeed, it is well known that blade lead-lag produces increased phase lag at high frequency, in the same frequency range where flapping effects occur [62], and that control rate gains are primarily limited by lead-lag-body coupling [62, 63]. Now, in terms of blade flap-lag modeling, a foundational contribution was given in [59], where derivations of the coupled flap-lag equations of motion for a rigid articulated rotor, for the (F-L-P), (F-P-L), and (L-F-P) sequences, was laid out. The purpose of our work is to present a model for a new hinge arrangement, i.e. the (P-L-F) sequence, which is much more useful for modeling the rotor dynamics of a small-scale helicopter. The equations presented in the sequel (obtained by the Lagrangian method [64]) are valid for a single articulated rotor with hinge springs and viscous dampers. Compared to [59] our approach retains all three hinges physically separated and works also for both ClockWise (CW) and Counter-ClockWise (CCW) rotating main rotors. Further, full coupling between vehicle and blade dynamics is modeled. Now from Lagrangian theory, we have

$$\frac{d}{dt} \left(\frac{\partial K_E}{\partial \dot{\zeta}_{bl}} \right) - \frac{\partial K_E}{\partial \zeta_{bl}} = Q_{\zeta_{bl}} \quad (25a)$$

$$\frac{d}{dt} \left(\frac{\partial K_E}{\partial \dot{\beta}_{bl}} \right) - \frac{\partial K_E}{\partial \beta_{bl}} = Q_{\beta_{bl}} \quad (25b)$$

with K_E the kinetic energy of a blade, β_{bl} , ζ_{bl} , blade flap and lag angles, and $Q_{\beta_{bl}}$, $Q_{\zeta_{bl}}$, the generalized forces. These latter include the effect of gravity, aerodynamics, and spring damping and stiffness, and are given by

$$Q_{\zeta_{bl}} = Q_{\zeta_{bl},G} + Q_{\zeta_{bl},A} + Q_{\zeta_{bl},D} + Q_{\zeta_{bl},S} \quad (26a)$$

$$Q_{\beta_{bl}} = Q_{\beta_{bl},G} + Q_{\beta_{bl},A} + Q_{\beta_{bl},D} + Q_{\beta_{bl},S} \quad (26b)$$

The kinetic energy of a single rotor blade is given by

$$K_E = \frac{1}{2} \int_0^{R_{bl}} \mathbf{V}_{I,P_{dm}}^{HB} \cdot \mathbf{V}_{I,P_{dm}}^{HB} dm \quad (27)$$

with $\mathbf{V}_{I,P_{dm}}^{HB}$ computed in Eqn. (18), and the limits of integration are from the flap hinge, to the blade tip. The kinetic energy inboard of the flap hinge is neglected in our model since assumed small in the case of small-scale UAVs. We provide next the procedure for the blade lead-lag equations Eqn. (25a), the blade flap equations Eqn. (25b) follow a similar reasoning and are thus omitted. Now we rewrite the first term on the Left-Hand-Side (LHS) of Eqn. (25a) as

$$\frac{d}{dt} \left(\frac{\partial K_E}{\partial \dot{\zeta}_{bl}} \right) = \frac{d}{dt} \left(\frac{\partial}{\partial \dot{\zeta}_{bl}} \frac{1}{2} \int_0^{R_{bl}} \mathbf{V}_{I,P_{dm}}^{HB \top} \cdot \mathbf{V}_{I,P_{dm}}^{HB} dm \right) \quad (28)$$

And since the limits of integration are constant, Eqn. (28) is equivalent to (using Leibniz's integral rule)

$$\frac{1}{2} \int_0^{R_{bl}} \frac{d}{dt} \frac{\partial}{\partial \dot{\zeta}_{bl}} \left(\mathbf{V}_{I,P_{dm}}^{HB \top} \cdot \mathbf{V}_{I,P_{dm}}^{HB} \right) dm \quad (29)$$

Next using the chain rule, Eqn. (29) is equivalent to

$$\frac{1}{2} \int_0^{R_{bl}} \frac{d}{dt} \left(2 \mathbf{V}_{I,P_{dm}}^{HB \top} \cdot \frac{\partial}{\partial \dot{\zeta}_{bl}} \mathbf{V}_{I,P_{dm}}^{HB} \right) dm = \int_0^{R_{bl}} \left[\mathbf{V}_{I,P_{dm}}^{HB \top} \cdot \left(\frac{d}{dt} \frac{\partial}{\partial \dot{\zeta}_{bl}} \mathbf{V}_{I,P_{dm}}^I \right)^{HB} + \left(\frac{d}{dt} \mathbf{V}_{I,P_{dm}}^I \right)^{HB} \cdot \frac{\partial}{\partial \dot{\zeta}_{bl}} \mathbf{V}_{I,P_{dm}}^{HB} \right] dm \quad (30)$$

with again the following convention for the time-derivatives: $\left(\frac{d}{dt} \frac{\partial}{\partial \dot{\zeta}_{bl}} \mathbf{V}_{I,P_{dm}}^I \right)^{HB}$ signifies the time-derivative, wrt inertial frame F_I , of vector $\frac{\partial}{\partial \dot{\zeta}_{bl}} \mathbf{V}_{I,P_{dm}}^I$, subsequently projected onto frame F_{HB} . Using Eqn. (16), these derivatives can also be expanded as follows

$$\left(\frac{d}{dt} \frac{\partial}{\partial \dot{\zeta}_{bl}} \mathbf{V}_{I,P_{dm}}^I \right)^{HB} = \left(\frac{d}{dt} \frac{\partial}{\partial \dot{\zeta}_{bl}} \mathbf{V}_{I,P_{dm}}^{HB} \right)^{HB} + \begin{pmatrix} p \\ q \\ r \end{pmatrix} \times \frac{\partial}{\partial \dot{\zeta}_{bl}} \mathbf{V}_{I,P_{dm}}^{HB} \quad (31)$$

$$\left(\frac{d}{dt} \mathbf{V}_{I,P_{dm}}^I \right)^{HB} = \left(\frac{d}{dt} \mathbf{V}_{I,P_{dm}}^{HB} \right)^{HB} + \begin{pmatrix} p \\ q \\ r \end{pmatrix} \times \left(\mathbf{V}_{I,P_{dm}}^I \right)^{HB} \quad (32)$$

Next, for the second term on the LHS of Eqn. (25a) we get

$$-\frac{\partial K_E}{\partial \zeta_{bl}} = -\frac{\partial}{\partial \zeta_{bl}} \frac{1}{2} \int_0^{R_{bl}} \mathbf{V}_{I,P_{dm}}^{HB \top} \cdot \mathbf{V}_{I,P_{dm}}^{HB} dm \quad (33)$$

Again since the limits of integration are constant, and using the chain rule, Eqn. (33) reduces to

$$-\frac{\partial K_E}{\partial \zeta_{bl}} = - \int_0^{R_{bl}} \mathbf{V}_{I,P_{dm}}^{HB \top} \cdot \frac{\partial}{\partial \zeta_{bl}} \mathbf{V}_{I,P_{dm}}^{HB} dm \quad (34)$$

Now, through the use of a symbolic math toolbox, an analytic expression for the LHS of Eqn. (25a) may readily be obtained, i.e. by utilizing the expression obtained for $\mathbf{V}_{I,P_{dm}}^{HB}$ in Eqn. (18) and inserting it, together with the derivatives $\frac{d}{dt} \mathbf{V}_{I,P_{dm}}^{HB}$, $\frac{\partial}{\partial \dot{\zeta}_{bl}} \mathbf{V}_{I,P_{dm}}^{HB}$, $\frac{\partial}{\partial \zeta_{bl}} \mathbf{V}_{I,P_{dm}}^{HB}$, into Eqn. (30), Eqn. (31), Eqn. (32), and Eqn. (34). The blade flap equation Eqn. (25b) follows a similar procedure, and will also require the computation of $\frac{\partial}{\partial \beta_{bl}} \mathbf{V}_{I,P_{dm}}^{HB}$ and $\frac{\partial}{\partial \dot{\beta}_{bl}} \mathbf{V}_{I,P_{dm}}^{HB}$. Finally, using a symbolic math toolbox, the combined equations Eqn. (25a) and Eqn. (25b) may be re-arranged as the following four-states nonlinear flap-lag equations of motion

$$\frac{d}{dt} \begin{pmatrix} \dot{\beta}_{bl} \\ \dot{\zeta}_{bl} \\ \beta_{bl} \\ \zeta_{bl} \end{pmatrix} = \mathbb{A}^{-1} \cdot \left(-\mathbb{B} \cdot \begin{pmatrix} \dot{\beta}_{bl} \\ \dot{\zeta}_{bl} \\ \beta_{bl} \\ \zeta_{bl} \end{pmatrix} + \begin{pmatrix} Q_{\beta_{bl}} - F_1 \\ Q_{\zeta_{bl}} - F_2 \\ 0 \\ 0 \end{pmatrix} \right) \quad (35)$$

with the following \mathbb{A} and \mathbb{B} matrices

$$\mathbb{A} = \begin{bmatrix} I_\beta & 0 & 0 & 0 \\ 0 & (e_F^2 \cdot M_{bl} + 2e_F \cdot C_0 + I_\beta) & 0 & 0 \\ 0 & 0 & 1 & 0 \\ 0 & 0 & 0 & 1 \end{bmatrix} \quad \mathbb{B} = \begin{bmatrix} 0 & B_{12} & 0 & 0 \\ B_{21} & 0 & 0 & 0 \\ -1 & 0 & 0 & 0 \\ 0 & -1 & 0 & 0 \end{bmatrix} \quad (36)$$

with M_{bl} , C_0 , and I_β defined as (refer also to the nomenclature)

$$M_{bl} = \int_0^{R_{bl}} dm \quad C_0 = \int_0^{R_{bl}} r_{dm} \cdot dm = M_{bl} \cdot \gamma_{G_{bl}} \quad I_\beta = \int_0^{R_{bl}} r_{dm}^2 \cdot dm = M_{bl} \cdot \frac{R_{bl}^2}{3} \quad (37)$$

We stress here that Eqn. (35) is a nonlinear representation since the scalars B_{12} and B_{21} in Eqn. (36), and F_1 , and F_2 in Eqn. (35) are (nonlinear) functions of $(\zeta_{bl}, \beta_{bl}, \zeta_{bl})$. Space restrictions preclude a reprint of the lengthy expressions B_{12} , B_{21} , F_1 , and F_2 , these can be consulted in Appendix E of [65].

3.4.1 Flap Angle as a Fourier Series

Blade motion is 2π periodic around the azimuth and may hence be expanded as an infinite Fourier series [54, 66]. Now for full-scale helicopters, it is well known that the magnitude of the flap second harmonic is less than 10% the magnitude of the flap first harmonic [34, 54]. We assume that this is also the case for small-scale helicopters and hence we neglect second and higher harmonics in the Fourier series. This gives

$$\beta_{bl}(\psi_{bl}) \simeq \beta_0 + \beta_{1c} \cos \psi_{bl} + \beta_{1s} \sin \psi_{bl} \quad (38)$$

with ψ_{bl} the blade azimuth angle. This harmonic representation of the blade motion defines the rotor Tip-Path-Plane (TPP), resulting in a so-called cone-shaped rotor. The non-periodic term β_0 describes the coning angle, and the coefficients of the first harmonic β_{1c} and β_{1s} describe the tilting of the rotor TPP, in the longitudinal and lateral directions respectively. All three angles may readily be obtained through standard least-squares [67]. Now in steady-state rotor operation, the flap coefficients β_0 , β_{1c} , β_{1s} may be considered constant over a 2π blade revolution. Obviously this solution would not be adequate for transient situations such as maneuvering [68], hence in our model we compute, for each new blade azimuth, the instantaneous TPP angles. With regard to TPP dynamics, three natural modes can be identified, i.e. the so-called coning, advancing, and regressing modes. In general, the regressing flapping mode is the most relevant when focusing on helicopter flight dynamics, as it is the lowest frequency mode of the three, and it has a tendency to couple into the fuselage modes [53, 62, 69].

3.4.2 Virtual Work and Virtual Displacements

The determination of the generalized forces $Q_{\zeta_{bl}}$, $Q_{\beta_{bl}}$ in Eqn. (26a) Eqn. (26b) requires the calculation of the virtual work of each individual external force, associated with each respective virtual flapping and lead-lag displacements [59]. Let $F_{X_i}, F_{Y_i}, F_{Z_i}$ be the components of the i^{th} external force \mathbf{F}_i , acting on blade element dm in frame F_{HB} , then the resulting elemental virtual work done by this force, due to the virtual flapping and lag displacements $\delta\beta_{bl}$ and $\delta\zeta_{bl}$, is given by

$$dW_i = F_{X_i} dx_{dm} + F_{Y_i} dy_{dm} + F_{Z_i} dz_{dm} \quad (39)$$

with

$$dx_{dm} = \frac{\partial x_{dm}}{\partial \beta_{bl}} \delta\beta_{bl} + \frac{\partial x_{dm}}{\partial \zeta_{bl}} \delta\zeta_{bl} \quad (40a)$$

$$dy_{dm} = \frac{\partial y_{dm}}{\partial \beta_{bl}} \delta\beta_{bl} + \frac{\partial y_{dm}}{\partial \zeta_{bl}} \delta\zeta_{bl} \quad (40b)$$

$$dz_{dm} = \frac{\partial z_{dm}}{\partial \beta_{bl}} \delta\beta_{bl} + \frac{\partial z_{dm}}{\partial \zeta_{bl}} \delta\zeta_{bl} \quad (40c)$$

Now summing up the elemental virtual work, over the appropriate blade span, results in the total virtual work W_i , due to external force \mathbf{F}_i , as

$$W_i = \int_0^{R_{bl}} \left(F_{X_i} \frac{\partial x_{dm}}{\partial \beta_{bl}} + F_{Y_i} \frac{\partial y_{dm}}{\partial \beta_{bl}} + F_{Z_i} \frac{\partial z_{dm}}{\partial \beta_{bl}} \right) \delta\beta_{bl} + \int_0^{R_{bl}} \left(F_{X_i} \frac{\partial x_{dm}}{\partial \zeta_{bl}} + F_{Y_i} \frac{\partial y_{dm}}{\partial \zeta_{bl}} + F_{Z_i} \frac{\partial z_{dm}}{\partial \zeta_{bl}} \right) \delta\zeta_{bl} \quad (41)$$

Which is set equivalent to

$$W_i = Q_{\beta_{bl},i} \cdot \partial \beta_{bl} + Q_{\zeta_{bl},i} \cdot \partial \zeta_{bl} \quad (42)$$

The virtual displacement, in frame F_{HB} , of a blade element dm , located at a distance r_{dm} outboard of the flap hinge, is obtained using Eqn. (40) and Eqn. (9) as follows

$$\begin{pmatrix} dx_{dm} \\ dy_{dm} \\ dz_{dm} \end{pmatrix}^{HB} = r_{dm} \cdot \mathbf{dP}_{\beta,r}^{HB} \cdot \partial \beta_{bl} + \left[\mathbf{dP}_{\zeta,r}^{HB} + r_{dm} \cdot \mathbf{dP}_{\zeta,r}^{HB} \right] \cdot \partial \zeta_{bl} \quad (43)$$

with

$$\mathbf{dP}_{\beta,r}^{HB} = \begin{pmatrix} \cos \psi_{bl} \cos \zeta_{bl} \sin \beta_{bl} + \sin \psi_{bl} \left(\cos \theta_{bl} \sin \zeta_{bl} \sin \beta_{bl} - \cos \beta_{bl} \sin \theta_{bl} \right) \\ \Gamma \cos \psi_{bl} \left(\cos \theta_{bl} \sin \zeta_{bl} \sin \beta_{bl} - \cos \beta_{bl} \sin \theta_{bl} \right) - \Gamma \sin \psi_{bl} \cos \zeta_{bl} \sin \beta_{bl} \\ - \cos \theta_{bl} \cos \beta_{bl} - \sin \zeta_{bl} \sin \theta_{bl} \sin \beta_{bl} \end{pmatrix} \quad (44)$$

$$\mathbf{dP}_{\zeta,r}^{HB} = e_F \begin{pmatrix} \left(\cos \psi_{bl} \sin \zeta_{bl} - \sin \psi_{bl} \cos \theta_{bl} \cos \zeta_{bl} \right) \\ -\Gamma \left(\cos \psi_{bl} \cos \theta_{bl} \cos \zeta_{bl} + \sin \psi_{bl} \sin \zeta_{bl} \right) \\ \cos \zeta_{bl} \sin \theta_{bl} \end{pmatrix} \quad (45)$$

$$\mathbf{dP}_{\zeta,r}^{HB} = \cos \beta_{bl} \frac{\mathbf{dP}_{\zeta,r}^{HB}}{e_F} \quad (46)$$

3.4.3 Generalized Forces (Gravity)

The gravity force acting on a blade element with mass dm can be expressed in F_{HB} as

$$\mathbf{F}_{G_{bl}}^{HB} = \mathbb{T}_{(HB)o} \begin{pmatrix} 0 \\ 0 \\ g \cdot dm \end{pmatrix}^o \quad (47)$$

with $\mathbb{T}_{(HB)o}$ the transformation from F_o to F_{HB} . Substituting Eqn. (47) and Eqn. (43) into Eqn. (41), the desired generalized forces due to gravity, outboard of the flap hinge, are obtained as follows

$$Q_{\zeta_{bl},G} = g \cdot \left(e_F \cdot M_{bl} + C_0 \cos \beta_{bl} \right) \cdot \left(A_1 \cos \psi_{bl} \sin \zeta_{bl} - A_1 \sin \psi_{bl} \cos \theta_{bl} \cos \zeta_{bl} - A_2 \Gamma \cos \psi_{bl} \cos \theta_{bl} \cos \zeta_{bl} - A_2 \Gamma \sin \psi_{bl} \sin \zeta_{bl} + A_3 \cos \zeta_{bl} \sin \theta_{bl} \right) \quad (48)$$

$$Q_{\beta_{bl},G} = g \cdot C_0 \cdot \left(A_1 \cos \psi_{bl} \cos \zeta_{bl} \sin \beta_{bl} + A_1 \sin \psi_{bl} \cos \theta_{bl} \sin \zeta_{bl} \sin \beta_{bl} - A_1 \sin \psi_{bl} \cos \beta_{bl} \sin \theta_{bl} + A_2 \Gamma \cos \psi_{bl} \cos \theta_{bl} \sin \zeta_{bl} \sin \beta_{bl} - A_2 \Gamma \cos \psi_{bl} \cos \beta_{bl} \sin \theta_{bl} - A_2 \Gamma \sin \psi_{bl} \cos \zeta_{bl} \sin \beta_{bl} - A_3 \cos \theta_{bl} \cos \beta_{bl} - A_3 \sin \zeta_{bl} \sin \theta_{bl} \sin \beta_{bl} \right) \quad (49)$$

using

$$A_1 = -\sin \theta \quad A_2 = \cos \theta \sin \phi \quad A_3 = \cos \theta \cos \phi \quad (50)$$

and M_{bl} and C_0 as defined in Eqn. (37).

3.4.4 Generalized Forces (Aerodynamic)

The aerodynamic velocity, i.e. velocity relative to the air, of a blade element dm , located at position P_{dm} , is defined by $\mathbf{V}_{a,P_{dm}}$. Projecting it onto the blade frame F_{bl} we get

$$\mathbf{V}_{a,P_{dm}}^{bl} = \mathbb{T}_{(bl)(HB)} \cdot \left(\mathbf{V}_{I,P_{dm}}^{HB} - \begin{pmatrix} 0 \\ 0 \\ v_i \end{pmatrix}^{HB} - \mathbb{T}_{(HB)E} \begin{pmatrix} u_w \\ v_w \\ w_w \end{pmatrix}^E \right) \quad (51)$$

with $\mathbf{V}_{I,P_{dm}}^{HB}$ defined in Eqn. (18), v_i the rotor induced velocity¹³ from Eqn. (65), $(u_w \ v_w \ w_w)^\top$ the components of the wind velocity vector usually available in frame F_E , and $\mathbb{T}_{(bl)(HB)}$ the rotation matrix from frame F_{HB} to frame F_{bl} . Now the section AOA of a blade element dm is defined by α_{bl} in the interval $[-\pi, +\pi]$ rad and, for each of the four quadrants, is readily computed from the arctangent of the x- and z- components of $\mathbf{V}_{a,P_{dm}}^{bl}$. Further, the elemental lift and drag forces of a blade segment of length dr_{dm} are given by

$$dL = \frac{1}{2} \cdot \rho \cdot \|\mathbf{V}_{a,P_{dm}}^{bl}\|^2 \cdot c_{l_{bl}} \cdot c_{bl} \cdot dr_{dm} \quad (52)$$

$$dD = \frac{1}{2} \cdot \rho \cdot \|\mathbf{V}_{a,P_{dm}}^{bl}\|^2 \cdot c_{d_{bl}} \cdot c_{bl} \cdot dr_{dm} \quad (53)$$

with the blade section lift and drag coefficients $c_{l_{bl}}$ and $c_{d_{bl}}$ given as tabulated functions of blade section AOA and Mach number M , and all other coefficients defined in the nomenclature. The elemental lift and drag forces can now be expressed in the blade frame F_{bl} , for each of the four AOA quadrants. For example, for the case of a CCW main rotor, with the AOA quadrant $\alpha_{bl} \in [0, +\pi/2]$ rad, we have

$$d\mathbf{L}^{bl} = dL \cdot \begin{pmatrix} \sin \alpha_{bl} \\ 0 \\ -\cos \alpha_{bl} \end{pmatrix} \quad (54)$$

$$d\mathbf{D}^{bl} = -dD \cdot \begin{pmatrix} \cos \alpha_{bl} \\ 0 \\ \sin \alpha_{bl} \end{pmatrix} \quad (55)$$

Coming back to the generalized aerodynamic forces, we can now express them as the sum of two contributions, one due to lift and one due to drag. For the lead-lag case in Eqn. (26a) we have $Q_{\zeta_{bl},A} = Q_{\zeta_{bl},AL} + Q_{\zeta_{bl},AD}$. Similarly for the flap case in Eqn. (26b) $Q_{\beta_{bl},A} = Q_{\beta_{bl},AL} + Q_{\beta_{bl},AD}$. Now keeping in mind Eqn. (41) and Eqn. (43), and using Eqn. (54) and Eqn. (55), we obtain

$$Q_{\zeta_{bl},AL} = \int_{r_c}^{B.R_{bl}} \left(\mathbb{T}_{(HB)(bl)} d\mathbf{L}^{bl} \right)^\top \cdot \left(d\mathbf{P}_{\zeta,\bar{r}}^{HB} + r_{dm} \cdot d\mathbf{P}_{\zeta,r}^{HB} \right) \cdot dr_{dm} \quad (56)$$

$$Q_{\zeta_{bl},AD} = \int_{r_c}^{R_{bl}} \left(\mathbb{T}_{(HB)(bl)} d\mathbf{D}^{bl} \right)^\top \cdot \left(d\mathbf{P}_{\zeta,\bar{r}}^{HB} + r_{dm} \cdot d\mathbf{P}_{\zeta,r}^{HB} \right) \cdot dr_{dm} \quad (57)$$

$$Q_{\beta_{bl},AL} = \int_{r_c}^{B.R_{bl}} \left(\mathbb{T}_{(HB)(bl)} d\mathbf{L}^{bl} \right)^\top \cdot d\mathbf{P}_{\beta,r}^{HB} \cdot r_{dm} \cdot dr_{dm} \quad (58)$$

¹³Strictly speaking the induced velocity is perpendicular to the Tip-Path-Plane (TPP). However since we make the assumption of small tilt angles, as to simplify the model, we consider here an induced velocity perpendicular to the Hub-Body frame F_{HB} .

$$Q_{\beta_{bl},AD} = \int_{r_c}^{R_{bl}} \left(\mathbb{T}_{(HB)(bl)} \mathbf{dD}^{bl} \right)^\top \cdot \mathbf{dP}_{\beta,r}^{HB} \cdot r_{dm} \cdot dr_{dm} \quad (59)$$

For the lift contributions $Q_{\zeta_{bl},AL}$ and $Q_{\beta_{bl},AL}$, the integration is performed from the blade root cutout r_c to a value denoted as $B.R_{bl}$, this latter accounts for blade tip loss [68]. Next by plugging Eqn. (44), Eqn. (46), Eqn. (45), Eqn. (54), and Eqn. (55), into Eqn. (56)–Eqn. (59), one can derive final expressions for the generalized aerodynamic forces. Providing analytical expressions for Eqn. (56)–Eqn. (59) represents a rather tedious task, even more so for twisted blades¹⁴ for which the blade pitch will also be function of the blade section length r_{dm} . Therefore we have opted for a numerical evaluation of these expressions, as is often done in flight dynamics codes [70]. Here Gaussian quadrature integration was implemented, using a low order (fifth order) Legendre polynomial scheme [71, 72].

3.4.5 Generalized Forces (Hub Damping and Spring Restraints)

We consider hinge springs with viscous dampers. The generalized forces corresponding to the spring dampers can be obtained directly from the potential energy of the dampers dissipation functions [59, 64] as

$$Q_{\zeta_{bl},D} = -K_{D\zeta} \cdot \dot{\zeta}_{bl} \quad Q_{\beta_{bl},D} = -K_{D\beta} \cdot \dot{\beta}_{bl} \quad (60)$$

Similarly the generalized forces corresponding to the spring restraints can be obtained directly from the potential energy of the hub springs [59, 64] as

$$Q_{\zeta_{bl},S} = -K_{S\zeta} \cdot \zeta_{bl} \quad Q_{\beta_{bl},S} = -K_{S\beta} \cdot \beta_{bl} \quad (61)$$

3.5 Rotor Inflow

At the heart of the helicopter aerodynamics are the induced velocities, i.e. induced by rotor blade motion, at and near the main rotor [73]. They contribute to the local blade incidence and local dynamic pressure, and can be divided into two categories, static and dynamic inflow models. For low-bandwidth maneuvering applications, such as trim calculations or flying-qualities investigations, the dynamic effects of the interaction of the air mass with the vehicle may be deemed negligible, hence static inflow models may be acceptable [73]. But for high bandwidth applications, dynamic interactions between the inflow dynamics and the blade motion must be considered. Conjointly dynamic inflow models can be divided into two unsteady categories¹⁵: the Pitt-Peters dynamic inflow [77–80], and the Peters-He finite-state wake model [81–83]. The finite-state wake model is a more comprehensive theory than dynamic inflow, not limited in harmonics and allowing to account for nonlinear radial inflow distributions. This sophisticated model is particularly attractive when rotor vibration and aeroelasticity need to be analyzed [84]. But with respect to flight dynamics applications, we assume that it is sufficient to consider the normal component of the inflow at the rotor, i.e. the rotor induced downwash [49]. Further, for such applications, it is reported in [84] that the Peters-He model is not remarkably better than the Pitt-Peters formulation. Since our primary interest is flight dynamics, we choose to implement the more straightforward Pitt-Peters model [77, 79], with a correction for flight into the VRS from [85]. Note that, if required, additional enhancements could also be made by including a pseudo-harmonic term to model VRS thrust fluctuations as in [86]. Concerning wake bending during maneuvering flight¹⁶, we choose at first not to implement it, as to lower model complexity. Finally, for the aspect of ground effect, only a static ground effect has been accounted for, by a correction factor applied to the non-dimensional total velocity at the rotor disk center.

The induced inflow model implemented in our paper is based upon [79], and is assumed to have the following variations in the TPP wind-axis coordinates (see [79] for further details on TPP wind-axis coordinates)

$$\frac{d}{dt} \begin{pmatrix} \lambda_0 \\ \lambda_s \\ \lambda_c \end{pmatrix} = \Omega_{MR} \cdot \mathbb{M}^{-1} \cdot \left(-(\mathbb{L}_1 \cdot \mathbb{L}_2)^{-1} \cdot \begin{pmatrix} \lambda_0 \\ \lambda_s \\ \lambda_c \end{pmatrix} + \mathbf{C}_{aero} \right) \quad (62)$$

where the main rotor RPM Ω_{MR} has been added here in front of the RHS of Eqn. (62) since the original expressions of the Pitt-Peters model are in non-dimensional time (see also [81]). The subscript $(\cdot)_{aero}$ in the forcing function \mathbf{C}_{aero} indicates

¹⁴Although in our case the helicopter UAV blades have zero twist.

¹⁵Although recent advances in computing power and methodology have made it foreseeable to add a third category, namely that of detailed free-wake models that may be run in real-time for flight dynamics applications [74–76].

¹⁶Wake bending may significantly change the inflow distribution over the rotor, resulting in a sign reversal in the off-axis response [87–89], for which interesting implementation results can be found in [16, 90, 91].

that only aerodynamic contributions are considered, with $\mathbf{C}_{aero} = (C_T \ -C_L \ -C_M)_{aero}^T$, and C_T, C_L, C_M , the instantaneous main rotor thrust, roll, and pitching moment coefficients respectively, in the TPP wind-axis system. C_T is readily obtained from Eqn. (66), whereas C_L and C_M are simply derived from the forces Eqn. (66) times their respective moment arms. Next matrices \mathbb{M} and \mathbb{L}_1 are defined from [79] as

$$\mathbb{M} = \begin{bmatrix} \frac{8}{3\pi} & 0 & 0 \\ 0 & \frac{16}{45\pi} & 0 \\ 0 & 0 & \frac{16}{45\pi} \end{bmatrix} \quad \mathbb{L}_1 = \begin{bmatrix} \frac{1}{2} & 0 & \frac{-15\pi}{64} \sqrt{\frac{1-\sin\alpha}{1+\sin\alpha}} \\ 0 & \frac{4}{1+\sin\alpha} & 0 \\ \frac{15\pi}{64} \sqrt{\frac{1-\sin\alpha}{1+\sin\alpha}} & 0 & \frac{4\sin\alpha}{1+\sin\alpha} \end{bmatrix} \quad (63)$$

where α represents the wake angle with respect to the rotor disk [79]. Further matrix \mathbb{L}_2 is given by

$$\mathbb{L}_2 = \begin{bmatrix} (G_{eff} \cdot V_T)^{-1} & 0 & 0 \\ 0 & V_M^{-1} & 0 \\ 0 & 0 & V_M^{-1} \end{bmatrix} \quad (64)$$

with V_T the total velocity through the rotor disk, V_M the momentum theory mass flow parameter, and G_{eff} the static ground effect factor added as a correction to V_T . The expressions for V_T and V_M can be found in [85], although simpler expressions also exist in [79]. However the former include a correction for flight into the VRS and hence are more attractive. The G_{eff} coefficient is based upon the expression found in [68]. Finally the main rotor induced velocity v_i is computed as follows [92]: 1) solve Eqn. (62); 2) rotate the obtained inflow from the TPP wind-axis to the TPP axis (see [79]); and 3) use these expressions to compute v_i in Eqn. (65)

$$v_i = V_{ref} \cdot \left(\lambda_0 + \lambda_s \cdot \frac{r_{dm}}{R_{rot}} \cdot \sin\psi_{bl} + \lambda_c \cdot \frac{r_{dm}}{R_{rot}} \cdot \cos\psi_{bl} \right) \quad (65)$$

3.6 Forces and Moments

For the rotor forces, the procedure consists in simulating the forces of each individual blade. This process is repeated at each new blade azimuth position—rather than averaging the results over one revolution—in order to recreate the N_b/Rev flapping vibration (which may be useful when validating a complete auto-pilot system in a hardware in the loop simulation environment). The rotor forces are subdivided into three contributions: 1) aerodynamic lift and drag; 2) inertial; and 3) centrifugal forces. The aerodynamic forces $\mathbf{F}_{MR_a}^{HB}$ are obtained by integrating the elementary lift and drag forces Eqn. (54) and Eqn. (55) over the blade span

$$\mathbf{F}_{MR_a}^{HB} = \int_{r_c}^{R_{bl}} \mathbb{T}_{(HB)(bl)} \mathbf{dL}^{bl} \cdot dr_{dm} + \int_{r_c}^{R_{bl}} \mathbb{T}_{(HB)(bl)} \mathbf{dD}^{bl} \cdot dr_{dm} \quad (66)$$

where the integrations are done numerically as in Eqn. (56)–Eqn. (59). The inertial forces $\mathbf{F}_{MR_i}^{HB}$, due to flap and lag, are approximated, from expressions in [66], as follows

$$\mathbf{F}_{MR_i}^{HB} = \begin{bmatrix} 1 & 0 & 0 \\ 0 & 1 & 0 \\ 0 & 0 & 0 \end{bmatrix} \cdot \mathbb{T}_{(HB)6} \cdot \begin{pmatrix} -M_{bl}\eta_\zeta \ddot{\zeta}_{bl} \\ 0 \\ -M_{bl}\eta_\beta \ddot{\beta}_{bl} \end{pmatrix} \quad (67)$$

Centrifugal forces $\mathbf{F}_{MR_c}^{HB}$ are approximated, from [66], as

$$\mathbf{F}_{MR_c}^{HB} = \begin{bmatrix} 1 & 0 & 0 \\ 0 & 1 & 0 \\ 0 & 0 & 0 \end{bmatrix} \cdot \mathbb{T}_{(HB)6} \cdot \begin{pmatrix} 0 \\ \frac{1}{2} M_{bl} \Omega_{MR}^2 R_{bl}^2 \\ 0 \end{pmatrix} \quad (68)$$

Finally, for the total main rotor forces we have $\mathbf{F}_{MR}^b = \mathbb{T}_{b(HB)} \cdot (\mathbf{F}_{MR_a}^{HB} + \mathbf{F}_{MR_i}^{HB} + \mathbf{F}_{MR_c}^{HB})$, with $\mathbb{T}_{b(HB)} = \mathbb{I}$, since, as mentioned earlier, rotor shaft tilt-angles are zero on our helicopter UAV. For the rotor moments, they include contributions from six different sources: 1) aerodynamics $\mathbf{M}_{MR_a}^{HB}$; 2) inertial loads $\mathbf{M}_{MR_i}^{HB}$; 3) centrifugal loads $\mathbf{M}_{MR_c}^{HB}$; 4) flap hinge stiffness $\mathbf{M}_{MR_{stif}}^{HB}$;

5) lag hinge damping $\mathbf{M}_{MR_{damp}}^{HB}$; and 6) due to airfoil camber $\mathbf{M}_{MR_{camber}}^{HB}$. The last two are neglected since assumed very small for small-scale helicopter rotors/blades. The first three are simply computed by considering the forces Eqn. (66)–Eqn. (68) times their respective moment arms. For the flap hinge stiffness, it is derived from [66] as

$$\mathbf{M}_{MR_{stif}}^{HB} = -\frac{1}{1 - \frac{e_P + e_L + e_F}{R_{rot}}} \cdot \frac{N_b \cdot K_{S\beta}}{2} \begin{pmatrix} \Gamma\beta_{1s} \\ \beta_{1c} \\ 0 \end{pmatrix} \quad (69)$$

3.7 Rotor RPM Dynamics

The main rotor RPM dynamics is related to the available and required power by [57]

$$N_b \cdot I_b \cdot \Omega_{MR} \cdot \dot{\Omega}_{MR} = P_{shaft} - P_{req} \quad (70)$$

with P_{shaft} the available shaft power, and P_{req} the required power to keep the vehicle aloft. This latter is the sum of main rotor induced and profile power, tail rotor induced and profile power, power plant transmission losses, vehicle parasite power (i.e. drag due to fuselage, landing skids, rotor hub, etc), and finally main rotor, tail rotor, and fuselage aerodynamic interference losses. Considering the case of autorotation following an engine failure, a first-order response in P_{shaft} is generally assumed to represent the power decay, we have

$$\dot{P}_{shaft} = -\frac{P_{shaft}}{\tau_p} \quad (71)$$

with τ_p a to-be-identified time constant. For the required power P_{req} , we simplify the model by only considering the contributions from the main rotor as

$$P_{MR} = M_{z MR_a}^{HB} \cdot \Omega_{MR} \quad (72)$$

with $M_{z MR_a}^{HB}$ being the z- component of the aerodynamics moment $\mathbf{M}_{MR_a}^{HB}$ (this latter being referenced in the previous paragraph). If, at engine failure, we were to assume an instantaneous power loss $P_{shaft} = 0$, then from Eqn. (70) and Eqn. (72) we obtain

$$\dot{\Omega}_{MR} = -\frac{M_{z MR_a}^{HB}}{N_b \cdot I_b} \quad (73)$$

4 Tail Rotor

The tail rotor is a powerful design solution for torque balance, directional stability and control of helicopters. We have implemented here a standard Bailey type model [93], as is done in among others [67, 94, 95].

4.1 Assumptions

Structural simplifications

1. The blade has zero twist, constant chord, zero sweep, and has constant thickness ratio. The blade is also rigid, hence torsion is neglected.

Aerodynamics simplifications

1. Linear lift with constant lift curve slope, and uniform induced flow over the rotor are assumed.
2. Aerodynamic interference effects from the main rotor is neglected, although this may well be an oversimplification, for some flight conditions [96, 97]. Similarly, the aerodynamic interference from the vertical tail (due to blockage) is also neglected.
3. Compressibility, blade stall, and viscous flow effects are also disregarded.

Dynamical simplifications

1. Blade dynamics is disregarded, and simplified inflow dynamics is considered. Unsteady effects are neglected.

4.2 Forces and Moments

The theory we apply here is based on the work done by Bailey in [93], implemented among others in [67, 94]. The model given in this paper is a simplified approach of the Bailey model. First, the total tail rotor blade pitch $\tilde{\theta}_{TR}$ is given by

$$\tilde{\theta}_{TR} = \theta_{TR} - T_{TR} \frac{\partial \beta_{0TR}}{\partial T_{TR}} \tan \delta_{3TR} + \theta_{bias_{TR}} \quad (74)$$

with θ_{TR} the tail rotor control input, and all other coefficients defined in the nomenclature, except for T_{TR} defined in Eqn. (79). The Bailey coefficients are given next by

$$t_1 = \frac{B_{TR}^2}{2} + \frac{\mu_{TRxy}^2}{4} \quad (75a)$$

$$t_2 = \frac{B_{TR}^3}{3} + \frac{B_{TR} \mu_{TRxy}^2}{2} \quad (75b)$$

with B_{TR} the tip loss factor and μ_{TRxy} defined in the sequel. Now, assuming zero twist for the tail rotor blades, the downwash at the tail rotor is derived using momentum theory as follows

$$\lambda_{dw} = \frac{c_{l(0,TR)} \sigma_{TR}}{2} \left(\frac{\mu_{TRz} t_1 + \tilde{\theta}_{TR} t_2}{2 \sqrt{\mu_{TRx}^2 + \mu_{TRY}^2 + \lambda_{TR}^2} + \frac{c_{l(0,TR)} \sigma_{TR}}{2} t_1} \right) \quad (76)$$

with λ_{TR} the total tail rotor inflow, $\mu_{TRxy} = \sqrt{\mu_{TRx}^2 + \mu_{TRY}^2}$ and μ_{TRz} non-dimensional velocities in the tail rotor frame (see [67] for details of the tail rotor frame and the Bailey model), and the remaining coefficients defined in the nomenclature. The total tail rotor inflow λ_{TR} is further given by

$$\lambda_{TR} = \lambda_{dw} - \mu_{TRz} \quad (77)$$

where it is common practice to iterate between Eqn. (76) and Eqn. (77) until convergence within a reasonable tolerance. Then, the tail rotor thrust is given by [67]

$$\mathbf{F}_{TR}^b = \begin{pmatrix} 0 \\ \Gamma \cdot T_{TR} \\ 0 \end{pmatrix} \quad (78)$$

with

$$T_{TR} = 2 \cdot \lambda_{dw} \cdot \sqrt{\mu_{TRxy}^2 + \lambda_{TR}^2} \cdot \rho \cdot \pi \cdot \left(\Omega_{TR} \cdot R_{rotTR}^2 \right)^2 \quad (79)$$

Next, the tail rotor moments are primarily due to the rotor force times the respective moment arms (where we neglect any sideways rotor offset in the y - direction). For completeness, we also add the rotor torque acting on the pitch axis [66]

$$\mathbf{M}_{TR}^b = \begin{pmatrix} x_{TR} \\ 0 \\ z_{TR} \end{pmatrix}^b \times \mathbf{F}_{TR}^b + \begin{pmatrix} 0 \\ \sigma_{TR} \cdot C D_{TR} / 8 \cdot (1 + 4.6 \mu_{TRxy}^2) \cdot \rho \cdot \pi \cdot \Omega_{TR}^2 \cdot R_{rotTR}^5 \\ 0 \end{pmatrix}^b \quad (80)$$

5 Fuselage

In the general case, the flow around the fuselage is rather complex, and is characterized by strong nonlinearities, unsteady separation effects, and distortions due to the influence of the main rotor wake [49]. For low speed sideways flight, the important fuselage characteristics are the sideforce, vertical drag, and yawing moment; whereas in forward flight, the important characteristics include drag, and pitching and yawing moments variations with incidence and sideslip [49]. The fuselage rolling moment is usually small, except for configurations with deep hulls where the fuselage aerodynamic center may be significantly below the vehicle CG [49], see also [33, 98] for additional information.

5.1 Assumptions

Aerodynamics Simplifications

1. Fuselage aerodynamic center is collocated with vehicle CG. Further, only steady airloads effects are considered.
2. Effect of rotor downwash on fuselage is neglected. It can however be modeled as in [99], using a polynomial in wake skew angle, where the polynomial coefficients need to be fit from flight data [100].

5.2 Forces and Moments

The fuselage aerodynamic velocity, at its aerodynamic center, in the body frame F_b , is given by

$$\mathbf{V}_{a,Fus}^b = \begin{pmatrix} u + q.z_{Fus} - r.y_{Fus} \\ v - p.z_{Fus} + r.x_{Fus} \\ w + p.y_{Fus} - q.x_{Fus} \end{pmatrix}^b - \mathbb{T}_{(HB)E} \begin{pmatrix} u_w \\ v_w \\ w_w \end{pmatrix}^E \quad (81)$$

Now the fuselage model is based upon aerodynamic lift and drag coefficients, which are tabulated as a function of airflow AOA α_{Fus} and sideslip β_{Fus} angles [1]. These angles are readily computed from the x -, y -, and z - components of $\mathbf{V}_{a,Fus}^b$. The fuselage forces in the body frame F_b are

$$\mathbf{F}_{Fus}^b = \begin{pmatrix} q_{Fus} \cdot C_{x_{Fus}}^b(\alpha_{Fus}, \beta_{Fus}) \\ q_{Fus} \cdot C_{y_{Fus}}^b(\alpha_{Fus}, \beta_{Fus}) \\ q_{Fus} \cdot C_{z_{Fus}}^b(\alpha_{Fus}, \beta_{Fus}) \end{pmatrix} \quad (82)$$

with $q_{Fus} = 1/2 \cdot \rho \cdot S_{ref_{Fus}} \cdot \|\mathbf{V}_{a,Fus}^b\|^2$. The moments are

$$\mathbf{M}_{Fus}^b = \begin{pmatrix} q_{Fus} \cdot M_{x_{Fus}}^b(\alpha_{Fus}, \beta_{Fus}) \cdot L_{ref_{Fus}} \\ q_{Fus} \cdot M_{y_{Fus}}^b(\alpha_{Fus}, \beta_{Fus}) \cdot L_{ref_{Fus}} \\ q_{Fus} \cdot M_{z_{Fus}}^b(\alpha_{Fus}, \beta_{Fus}) \cdot L_{ref_{Fus}} \end{pmatrix} \quad (83)$$

with the six aerodynamic coefficients $C_{x_{Fus}}(\cdot)$, $C_{y_{Fus}}(\cdot)$, $C_{z_{Fus}}(\cdot)$, $M_{x_{Fus}}(\cdot)$, $M_{y_{Fus}}(\cdot)$, and $M_{z_{Fus}}(\cdot)$ being tabulated as a function of airflow AOA α_{Fus} , and sideslip angle β_{Fus} . In our case, these lookup tables are obtained by scaling-down a full-size, Bo-105 helicopter, fuselage aerodynamic model.

6 Vertical and Horizontal Tails

The role of the vertical tail is twofold: 1) in forward flight, it generates a sideforce and yawing moment, hence reducing the tail rotor thrust requirement, in order to increase the fatigue life of the tail rotor [49, 57]; and 2) during maneuvers, and during wind gusts, it provides yaw damping and stiffness, enhancing directional stability [49]. The role of the horizontal tail is also twofold: 1) in forward flight, it generates a trim load that reduces the main rotor fore-aft flapping; and 2) during maneuvers, and during wind gusts, it provides pitch damping and stiffness, enhancing pitch stability [49].

6.1 Assumptions

Aerodynamics Simplifications

1. The effect of main rotor downwash on both vertical and horizontal tails is neglected. It can however be modeled by using flat vortex wake theory [101] (valid for small sideslip angles), as presented in [70, 102], or it may be modeled as a polynomial in wake skew angle [99].

2. We neglect the erratic longitudinal trim shifts that may happen when the helicopter is transitioning from hover to forward flight [49, 57] (as the main rotor wake impinges on the tail surface).
3. The effect of the main rotor downwash on the tail boom is also neglected, but ought to be considered at low speed, since it may influence yaw damping [49].

6.2 Forces and Moments

The vertical and horizontal tails, for the case of small-scale helicopters, can simply be viewed as flat plate representations. The force equations are omitted since very similar to those of the fuselage, and the moments are simply derived from the forces times their respective moment arms.

7 Simulation Results

The purpose of this section is to evaluate, and validate, the open-loop behavior of our white-box helicopter mathematical model. Model validation can either be done by comparing the model's behavior with several recorded experimental data sets (i.e. flight tests), or by comparing the model's behavior with another simulation model, which is often a third-party, high-fidelity black-box model. In this paper, since flight data is not available, we opted for the second option, namely the use of the FLIGHTLAB¹⁷ [103] helicopter simulation environment. For aerospace systems, the model validation task generally involves the validation of, both, the static (trim) behavior as well as the dynamic response. A trim condition sets the helicopter in some, user-defined, steady-state (i.e. equilibrium) flight condition, by satisfying the system's equations of motion. Trim settings are often a prerequisite for stability analysis, vibration studies, and control system design. For instance, for linear control design, the linear models are generally obtained through analytical or numerical linearizations of the nonlinear model, around various trim conditions. For the validation of the dynamic behavior, either time-domain model responses or frequency-responses can be used.

In the sequel we will compare trim and time-response outputs of our MATLAB[®]-based model with those from a FLIGHTLAB model, for the case of a small-scale helicopter UAV. Both models include a main rotor, tail rotor, and fuselage. The modeled UAV is an instrumented, modified, Remote-Controlled (RC) Align T-REX helicopter, see Fig. 5, belonging to the flybarless two-bladed main rotor class, with a total mass of 7.75 kg, a main rotor radius of 0.9 m, a main rotor nominal angular velocity of 1350 RPM, a NACA 0015 main rotor airfoil, and with fuselage aerodynamic lookup tables obtained by scaling-down a full-size Bo105 helicopter fuselage aerodynamic model. The NACA 0015 and fuselage lookup tables are not reproduced here due to space constraints, however the remaining parameters have been listed in Table 1¹⁸. Note also that for this small-scale helicopter UAV, the Reynolds numbers vary approximately in the range $10^5 - 7 \cdot 10^5$, and hence these Reynolds numbers do not induce any particular limitations from an aerodynamic standpoint. For example, The Pitt-Peters dynamic inflow model (used in our main rotor model) has been successfully applied on systems with Reynolds numbers as low as 10^4 .

Our model is compared to an equivalent FLIGHTLAB model, with the parameters of the latter being set identical to the ones of Table 1. In addition, the options of the FLIGHTLAB model have been set as follows:

1. Articulated main rotor.
2. Blade element model and quasi-steady airloads.
3. Peters-He three-state inflow model, with no stall delay.
4. Bailey-type tail rotor.

7.1 Trim Results

A trim condition is equivalent to an equilibrium point of the nonlinear helicopter model [104], which can be thought of as a specific flight condition [20], in which the resultant forces and moments on the vehicle are equal to zero. For helicopters however, the concept of trim is more complicated than that of fixed-wing aircrafts [105], since a helicopter has components that rotate with respect to each other and with respect to the air mass. To circumvent this problem we developed a separate trim module, in the form of a constrained, nonlinear, optimization problem. At trim, the resultant forces and moments on the vehicle should be equal to zero, hence for the engine ON flight condition, the objective of the trim module is to set to zero the three vehicle inertial linear accelerations ($\dot{V}_N, \dot{V}_E, \dot{V}_Z$) and the three vehicle rotational accelerations ($\dot{p}, \dot{q}, \dot{r}$). On the other hand for the engine OFF flight condition (i.e. autorotation), the main rotor RPM Ω_{MR} is not fixed anymore as it is allowed to vary according to its own dynamics, hence the objective of the trim consists in setting to zero the previous six

¹⁷FLIGHTLAB is a state of the art modeling, analysis and real-time simulation tool, used world-wide to simulate helicopter flight dynamics.

¹⁸In this table the acronym *wrt* stands for *with respect to*.



Fig. 5: NLR's mini-UAV project (2012-2014) based on a modified Align TRex helicopter (courtesy of NLR)

Table 1: Align T-REX physical parameters for the environment, vehicle, and actuators

	Name	Parameter	Value	Unit
Environment	Air density	ρ	1.2367	kg/m^3
	Static temperature	T	273.15 + 15	K
	Specific heat ratio (air)	γ	1.4	
	Gas constant (air)	R	287.05	$J/kg.K$
	Gravity constant	g	9.812	m/s^2
Vehicle	Total mass	m	7.75	kg
	Inertia moment wrt x_b	A	0.2218	$kg.m^2$
	Inertia moment wrt y_b	B	0.5160	$kg.m^2$
	Inertia moment wrt z_b	C	0.3141	$kg.m^2$
	Inertia product wrt x_b	D	0	$kg.m^2$
	Inertia product wrt y_b	E	0.0014	$kg.m^2$
	Inertia product wrt z_b	F	0	$kg.m^2$
	X-pos. of Fus. CG wrt total CG	x_{Fus}	0	m
	Y-pos. of Fus. CG wrt total CG	y_{Fus}	0	m
Z-pos. of Fus. CG wrt total CG	z_{Fus}	0.017	m	
Actuators	MR collective	θ_0	$[-13,13].\pi/180$	rad
	MR lateral cyclic	θ_{1c}	$[-6,6].\pi/180$	rad
	MR longitudinal cyclic	θ_{1s}	$[-6,6].\pi/180$	rad
	TR collective	θ_{TR}	$[-20,20].\pi/180$	rad
	MR collective rate	$\dot{\theta}_0$	$[-52,52].\pi/180$	rad/s
	MR lateral cyclic rate	$\dot{\theta}_{1c}$	$[-52,52].\pi/180$	rad/s
	MR longitudinal cyclic rate	$\dot{\theta}_{1s}$	$[-52,52].\pi/180$	rad/s
	TR collective rate	$\dot{\theta}_{TR}$	$[-120,120].\pi/180$	rad/s

(Table 1 cont'd): Align T-REX physical parameters for the main rotor

	ClockWise direction of rotation	Γ	-1	
Main	Number of blades	N_b	2	
Rotor	Nominal angular velocity	$\Omega_{MR100\%}$	141.37	<i>rad/s</i>
(MR)	Rotor radius from hub	R_{rot}	0.9	<i>m</i>
	Blade mass	M_{bl}	0.2875	<i>kg</i>
	Spring restraint coef. due to flap	$K_{S\beta}$	162.69	<i>N.m/rad</i>
	Spring damping coef. due to flap	$K_{D\beta}$	0	<i>N.m.s/rad</i>
	Spring restraint coef. due to lag	$K_{S\zeta}$	0	<i>N.m/rad</i>
	Spring damping coef. due to lag	$K_{D\zeta}$	5	<i>N.m.s/rad</i>
	Offset distance	e_P	0.03	<i>m</i>
	Offset distance	e_L	0.06	<i>m</i>
	Offset distance	e_F	0.01	<i>m</i>
	Distance between hub and flap hinge	Δ_e	0.1	<i>m</i>
	Root cutout from flap hinge	r_c	0.0	<i>m</i>
	Blade chord	c_{bl}	0.064	<i>m</i>
	Blade twist at tip	θ_{wash}	0	<i>rad</i>
	Y-pos. blade CG wrt flap hinge	$y_{G_{bl}}$	0.4	<i>m</i>
	Swashplate phase angle	ψ_{PA}	0	<i>rad</i>
	Precone angle	β_P	0	<i>rad</i>
	Pitch-flap coupling ratio	$K_{(\theta\beta)}$	0	
	Pitch-lag coupling ratio	$K_{(\theta\zeta)}$	0	
	Tip loss factor	B	0.97	
	Airfoil lift coef.	$c_{l_{bl}}$	NACA0015	
	Airfoil drag coef.	$c_{d_{bl}}$	NACA0015	
	Airfoil pitching moment coef.	c_M	NACA0015	
	X-pos. of MR hub wrt total CG	x_H	0.01	<i>m</i>
	Y-pos. of MR hub wrt total CG	y_H	0	<i>m</i>
	Z-pos. of MR hub wrt total CG	z_H	-0.213	<i>m</i>

accelerations, defined for the engine ON case, together with an additional acceleration, namely the one related to main rotor RPM $\dot{\Omega}_{MR}$. This allows to find the steady-state autorotative flight conditions. Now, the variables that the trim algorithm is allowed to manipulate include the four control inputs $(\theta_0, \theta_{1c}, \theta_{1s}, \theta_{TR})$, and the vehicle roll and pitch angles (ϕ, θ) , since the latter two influence the projection of the gravity vector on the body frame. Besides, the set-point at which the equilibrium is computed has to be specified in the form of additional constraints, i.e. by assigning fixed values to the three vehicle inertial linear velocities (V_N, V_E, V_Z) , and the three vehicle rotational velocities (p, q, r) . Now regarding the dynamic inflow states $(\lambda_0, \lambda_s, \lambda_c)$, and the periodic states, i.e. blade flap and lag angles and velocities $(\beta_{bl}, \zeta_{bl}, \dot{\beta}_{bl}, \dot{\zeta}_{bl})$, these states are handled by time-marching the nonlinear helicopter model long enough until the transients have decayed. Finally, the remaining four states which include the three vehicle Cartesian position (x_N, x_E, x_Z) and the vehicle heading ψ are left free, since the position

(Table 1 cont'd): Align T-REX physical parameters for the tail rotor

Tail Rotor (TR)	Number of blades	N_{bTR}	2	
	Nominal angular velocity	$\Omega_{TR100\%}$	612.61	rad/s
	Rotor radius from rotor hub	R_{rotTR}	0.14	m
	Pitch-flap coupling	δ_{3TR}	0	rad
	Preset collective pitch bias	θ_{biasTR}	0	rad
	Partial coning angle wrt thrust	β_{0TR}	0	rad/N
	Tail blockage constant	b_{t1}	0.927	
	Transition velocity	v_{bl}	20	m/s
	Blade chord	c_{TR}	0.0316	m
	Tip loss factor	B_{TR}	0.92	
	Airfoil lift curve slope	$c_{l(0,TR)}$	5.92	rad^{-1}
	Blade drag coef.	CD_{TR}	0.0082	
	X-pos. of TR hub wrt total CG	x_{TR}	-1.015	m
	Y-pos. of TR hub wrt total CG	y_{TR}	-0.0575	m
Z-pos. of TR hub wrt total CG	z_{TR}	-0.034	m	

of the helicopter does not influence¹⁹ its dynamic behavior or stability. Our trim optimization is further based upon a Newton iteration scheme, similar to that of [95], which is simple to implement and has been widely used [106]. The Newton method guarantees quadratic local convergence, but is known to be sensitive to starting values.

We compare next our model trim results, for the engine ON case only²⁰, with those obtained with FLIGHTLAB. First, Table 2 gives the maximum absolute trim deviations, as a function of inertial linear velocities²¹ (V_N, V_E, V_Z), between our model and FLIGHTLAB, for the six trim variables, i.e. the four control inputs ($\theta_0, \theta_{1c}, \theta_{1s}, \theta_{TR}$) and roll and pitch angles (ϕ, θ). Table 2 has to be read in conjunction with Fig. 6–Fig. 11, where the trim results are plotted, along each motional axis. These motional axes are: longitudinal along V_N , lateral along V_E , vertical climb along V_Z ($V_Z > 0$), and vertical descent along V_Z ($V_Z < 0$). Basically, Fig. 6–Fig. 11 visualize the trim results for each motional axis at a time, i.e. by setting to zero the velocities along the remaining motional axes, whereas Table 2 compiles the worst-case data from Fig. 6–Fig. 11 by reporting the worst-case trim deviation, for each of the six trim variables, along each motional axis. In addition, Table 2 reports the results for the main rotor power P_{MR} , as this latter gives extra insight into the fidelity of our model.

We see that the maximum absolute deviations, between both models, for roll and pitch angles, are almost negligible, respectively below 1.5° and 0.7° , see Table 2. For the remaining variables, we also explore the relative deviations between both models. Regarding the control inputs, Table 3 gives their relative deviations in %, namely the maximum absolute deviations divided by the full actuator ranges. Overall, we see that the differences between both models are rather small, e.g. below 6 % for the Main Rotor (MR) collective θ_0 , below 5.5 % for the Tail Rotor (TR) collective θ_{TR} , below 3.5 % for the MR lateral cyclic θ_{1c} , and below 4.5 % for the MR longitudinal cyclic θ_{1s} . From Fig. 6, Fig. 7, and Fig. 8, we also see that the maximum relative trim deviation does not exceed 10 % for the main rotor power P_{MR} , for the longitudinal, lateral, and climb motions. However, we do notice, as can also be seen in Table 2, some higher discrepancies between both models in descending flight (particularly inside the VRS), where for instance the maximum relative trim deviation reaches 26 % for the main rotor power P_{MR} . This could probably indicate that both models are implementing distinct simulations of the induced rotor flow inside the VRS. The plot of the MR collective input θ_0 , on Fig. 9, reveals also the minimum power speed,

¹⁹Although strictly speaking this is not true in vertical flight, due to the ground effect when trimming near the ground, and due to changes in air density when trimming with a non-zero vertical velocity; however for the case of air density variations, these may be neglected when considering small-scale UAV applications, since the maximum flight altitude is generally below 150-200m above ground.

²⁰Comparison of our model with FLIGHTLAB, for the engine OFF case, is presented within the context of dynamic results.

²¹With V_Z positive up.

Table 2: Trim: Maximum absolute deviations between our model and FLIGHTLAB, for the engine ON case

Name	Maximum absolute deviations			
	longi- tudinal along V_N	lateral along V_E	climb along V_Z ($V_Z > 0$)	descent along V_Z ($V_Z < 0$)
Roll ϕ ($^\circ$)	1.0	0.7	1.5	0.5
Pitch θ ($^\circ$)	0.3	0.7	0.3	0.1
MR Collective θ_0 ($^\circ$)	0.5	0.5	0.5	1.5
TR Collective θ_{TR} ($^\circ$)	0.9	0.9	1.0	2.1
MR Lat. Cyclic θ_{1c} ($^\circ$)	0.4	0.04	0.04	0.05
MR Long. Cyclic θ_{1s} ($^\circ$)	0.1	0.5	0.1	0.3
MR Power P_{MR} (W)	59	58	76	156

Table 3: Trim: Maximum relative deviations between our model and FLIGHTLAB, for the control inputs in % of full actuator ranges, for the engine ON case

Name	Maximum relative deviations (in %)			
	longi- tudinal along V_N	lateral along V_E	climb along V_Z ($V_Z > 0$)	descent along V_Z ($V_Z < 0$)
MR Collective θ_0	1.9	1.9	1.9	5.8
TR Collective θ_{TR}	2.2	2.2	2.5	5.2
MR Lat. Cyclic θ_{1c}	3.3	0.3	0.3	0.4
MR Long. Cyclic θ_{1s}	0.8	4.2	0.8	2.5

sometimes called the *bucket speed*, predicted to be around 11–13 m/s by both models. From the MR power plot P_{MR} , in Fig. 7, we can also see that, as expected, for a CW main rotor for which the tail rotor thrust is oriented towards port-side (i.e. to the left), it takes more power for vehicle starboard flight (i.e. to the right) than for port-side flight. Finally, for our helicopter, the VRS region at $(V_N, V_E) = (0, 0)$ m/s is approximately defined by $-6 < V_Z < -3$ m/s (see also our discussion in [39]). Here, we clearly see from Fig. 8 and Fig. 11 that MR collective θ_0 and MR power P_{MR} , as expected, start to increase inside the VRS, e.g. compare their values at $V_Z = -4$ m/s vs. at $V_Z = -3$ m/s. Hence, more engine power is required from a VRS descent than from hover.

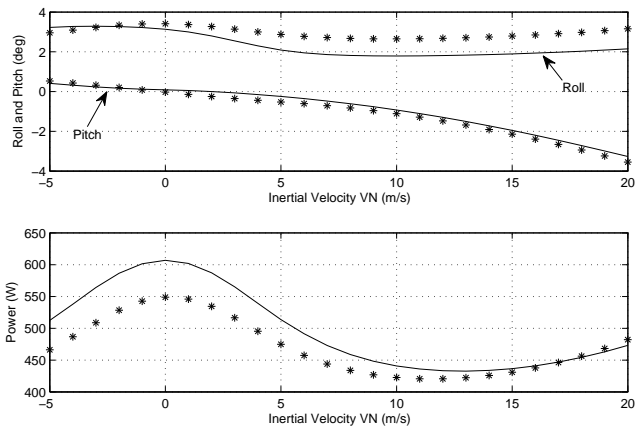


Fig. 6: Trim along inertial North velocity V_N : roll and pitch angles, and main rotor power (-FLIGHTLAB, * Our Model)

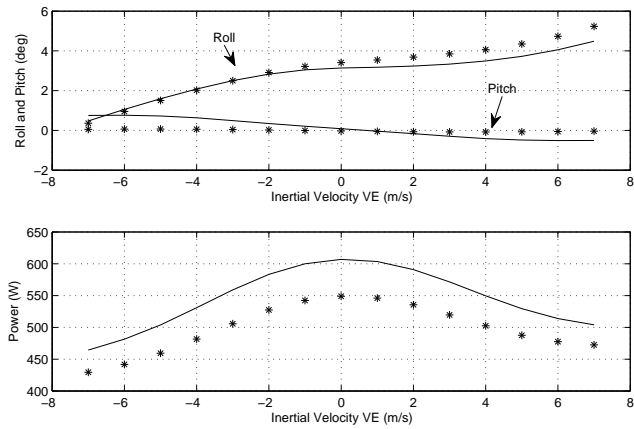


Fig. 7: Trim along inertial East velocity V_E : roll and pitch angles, and main rotor power (-FLIGHTLAB, * Our Model)

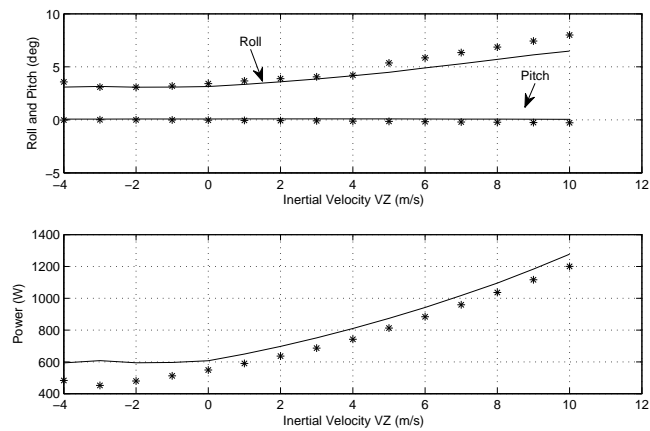


Fig. 8: Trim along inertial Vertical velocity V_Z : roll and pitch angles, and main rotor power (-FLIGHTLAB, * Our Model)

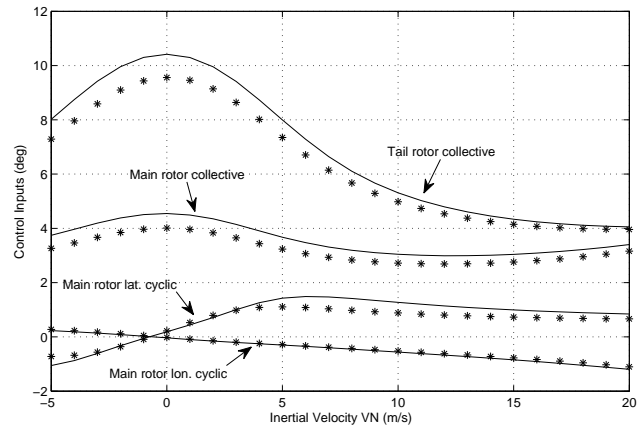


Fig. 9: Trim along inertial North velocity V_N : control inputs (-FLIGHTLAB, * Our Model)

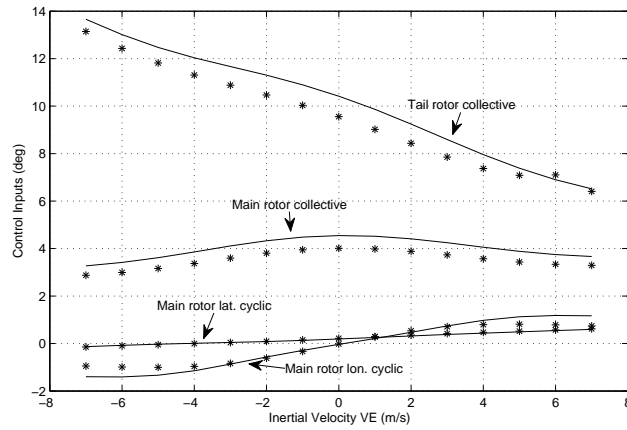


Fig. 10: Trim along inertial East velocity V_E : control inputs (-FLIGHTLAB, * Our Model)

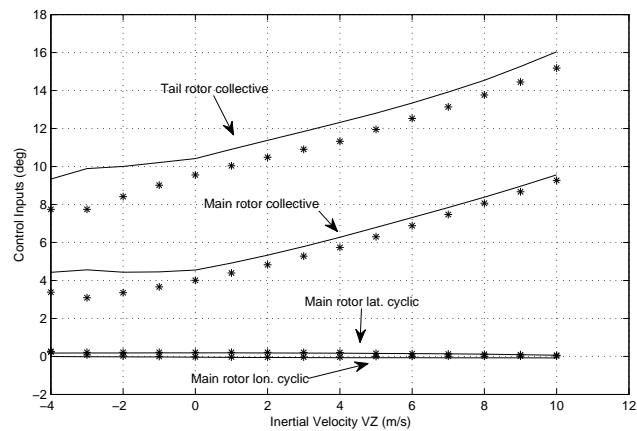


Fig. 11: Trim along inertial Vertical velocity V_Z : control inputs (-FLIGHTLAB, * Our Model)

7.2 Dynamic Results

For the dynamic response comparison, we compare the time histories of our model with those of FLIGHTLAB. Basically, the tests are set to evaluate the open-loop response of our helicopter model. Both models have a simulation time-step set equal to $1/24^{\text{th}}$ of a main rotor revolution²². First, the rotor is allowed to reach a steady-state condition during a time period of 1 s. (this is a purely software initialization matter, since the simulation starts with all states at zero). Then, for the following 3 s. we simultaneously apply sine-sweeps from 0 to 2 Hz on the four input channels²³, see Fig. 12. Next, we evaluate the responses of the following ten states: attitude angles (ϕ, θ, ψ) , body linear velocities (u, v, w) , body rotational velocities (p, q, r) , and MR RPM Ω_{MR} (the RPM is included for the autorotation case only). For a quantitative evaluation we use the Variance-Accounted-For (VAF), defined as: $\text{VAF} := 100\% \cdot \max\left(1 - \frac{\text{var}(\mathbf{x}_k - \tilde{\mathbf{x}}_k)}{\text{var}(\mathbf{x}_k)}, 0\right)$ with $\tilde{\mathbf{x}}_k$ one of the ten states in our model, and \mathbf{x}_k its FLIGHTLAB counterpart, see Table 4. The VAF is a widely used metric²⁴ in the realm of system identification²⁵

Three test cases are presented, all starting at an altitude of 30 m. The first two with the engine ON, and the third with the engine OFF. The first test case is run from the hover trim condition, see Fig. 13, where it can be seen that the overall fit with FLIGHTLAB is good to very good (see also Table 4). The second test case is run to evaluate the high speed flight condition, at $V_N = 10$ m/s, see Fig. 14, where we can see that the overall fit with FLIGHTLAB is again good, except for the low VAF value (of 28 %) reported for w (although the plot on the w channel is rather good, as can be seen in Fig. 14). Indeed, if the to-be-compared values are close to zero (as is here the case for w), the VAF metric will tend to artificially amplify any discrepancies. Naturally our model does not perfectly match FLIGHTLAB. To some extent the observed discrepancies, between both models, may originate from the fact that both models are built upon distinct modeling philosophies. For instance, for the derivation of the flap-lag dynamics as well as the computation of the rotor forces and moments, our model is based upon a white-box, first-principles approach, i.e. a closed-form representation of the system's behavior. On the contrary, FLIGHTLAB is based upon the so-called multi-body concept²⁶. For instance for the case of a FLIGHTLAB main rotor blade, this latter is split into N smaller bodies. Each body is undergoing a translational and rotational displacement, with the dynamic behavior of the complete system (here the complete blade, or multi-body system) resulting from the equilibrium of applied forces and the rate of change of momentum at each body. This difference in modeling philosophies will inevitably result in slight differences in, for instance, the magnitude of rotor forces and moments. Further, it is well known that even small variations in the computation of forces and moments will be integrated, over time, to large errors in velocities and positions²⁷. Besides, this effect gets exacerbated for highly unstable systems²⁸, which is generally the case of highly agile small-scale helicopters (on the one hand due to their very low inertia, and on the other due to the high rotor stiffness resulting in high rotor moments). To conclude, as can be seen from the last row in Table 4, the model's average VAF (over all states) is relatively high, i.e. in the range 66–85 %, and hence the realism of our model is considered to be of good quality.

8 Conclusion

The first building-block—towards the development of an autonomous helicopter system—has been presented, and can be characterized as a comprehensive modeling framework, particularly suited for small-scale flybarless helicopters. Comparisons with an equivalent FLIGHTLAB simulation shows that our model is valid for a range of flight conditions, including steep descent flights and autorotation. Hence, this model could potentially be used for several applications: 1) simulation of the flight dynamics of small-scale (articulated or hingeless) flybarless helicopters; 2) investigation of the coupling between flap/lag and inflow dynamics; as well as 3) providing a basis for model-based control design.

²²The default value in FLIGHTLAB.

²³The relatively short experiment time of 3 s. is explained by the short time-to-double amplitude, found to be in the range of 0.9–2.3 s., this latter being derived from the eigenvalues of local LTI models. Since the total experiment time is rather short, we chose to focus the model validation on its low-frequency behavior, hence the 2 Hz limit on the applied input signal.

²⁴VAF values above 75 % suggest a high-quality model, whereas values in the range 50–75 % would indicate an average-to-good model quality.

²⁵Note that, usually, the VAF is used in a parameter-estimation context where one tries to 'match' the outputs of a model with the data gathered from various experiments, or alternatively when one tries to 'match' the outputs of a lower-order model with those from a more complex, often higher-order, model. In our case, we simply use the VAF to compare two models, without any 'tuning' or 'fitting' of coefficients. Hence, in our case, the obtained VAF values tend to be lower than VAF values usually seen in a system identification context.

²⁶The multi-body concept may often be used to simulate the dynamic behavior of interconnected rigid and flexible bodies.

²⁷We note that the fit for test case 3 (autorotation) is better than the fit obtained for the first two test cases (with engine ON). The explanation being as follows: in autorotation, main and tail rotor collective have much lower values when compared to their engine ON values, and hence the generated aerodynamic forces are as well smaller in magnitude. Smaller aerodynamic forces also imply smaller discrepancies, in magnitude, between the forces computed by both models, resulting in smaller errors in velocities and positions when integrated over time.

²⁸This is also why system identification of unstable systems is most often done in closed-loop [107].

Table 4: Vehicle dynamic response to sine-sweeps on the four input channels: Variance-Accounted-For (VAF) by our model with respect to FLIGHTLAB

Name	VAF (%)		
	hover	$V_N = 10 \text{ m/s}$	steady-state autorotation $(V_N, V_Z) = (6, -6) \text{ m/s}$
Roll ϕ	51	76	86
Pitch θ	73	84	59
Yaw ψ	61	50	96
Long. velocity u	79	84	84
Lat. velocity v	62	91	96
Vertical velocity w	93	28	92
Roll rate p	67	45	76
Pitch rate q	43	68	77
Yaw rate r	95	70	97
MR RPM Ω_{MR}	N.A.	N.A.	82
Average over all states	69	66	85

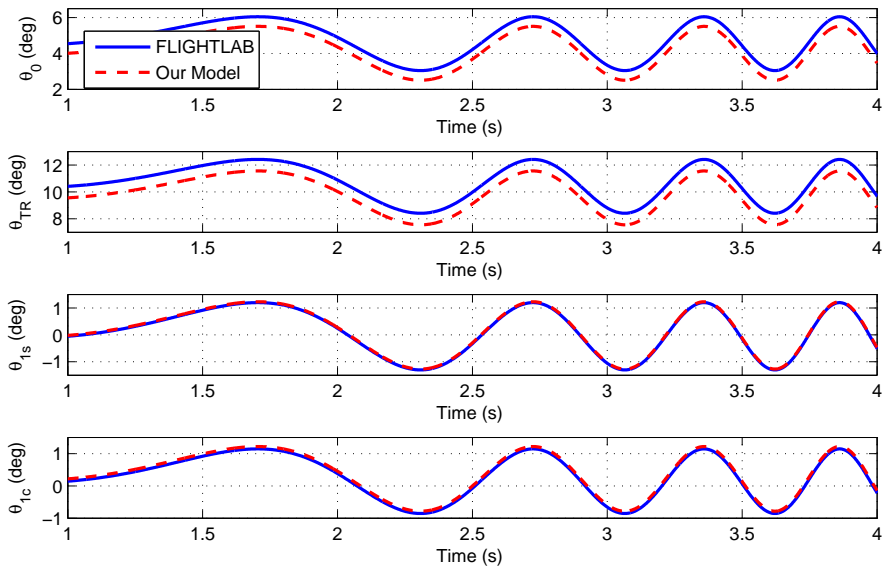


Fig. 12: Vehicle dynamics: sine-sweep inputs for test cases 1, 2, & 3 (—FLIGHTLAB, --Our Model)

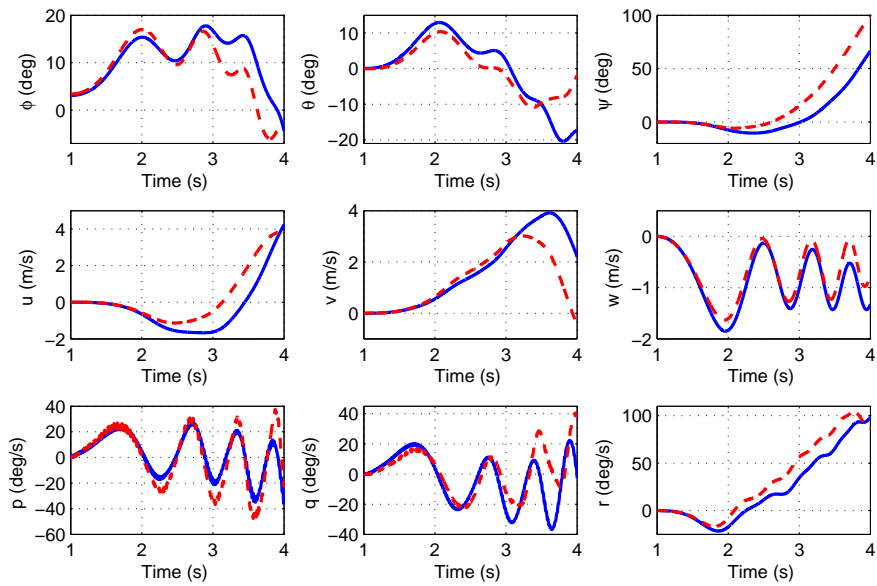


Fig. 13: Vehicle dynamics (test case 1): response to sine-sweep inputs from hover (-FLIGHTLAB, --Our Model)

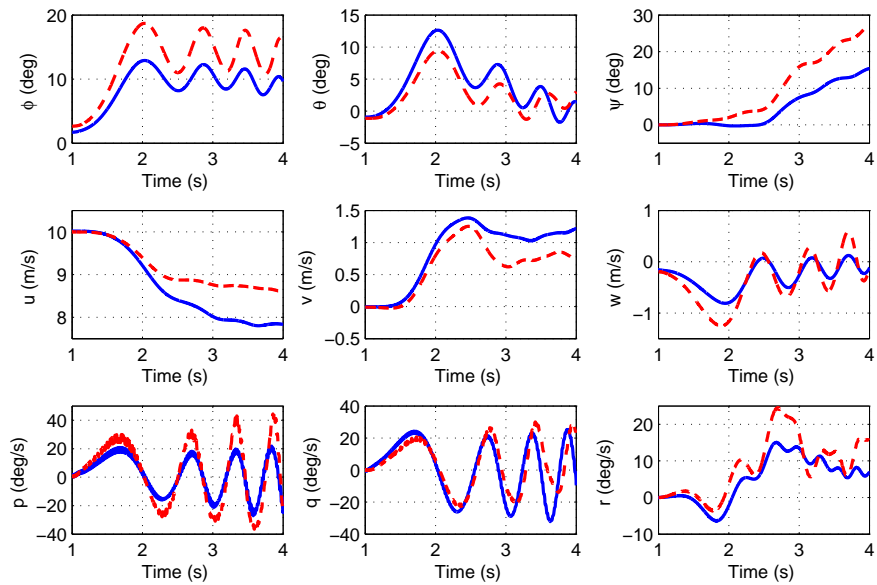


Fig. 14: Vehicle dynamics (test case 2): response to sine-sweep inputs from $V_N = 10 \text{ m/s}$ (-FLIGHTLAB, --Our Model)

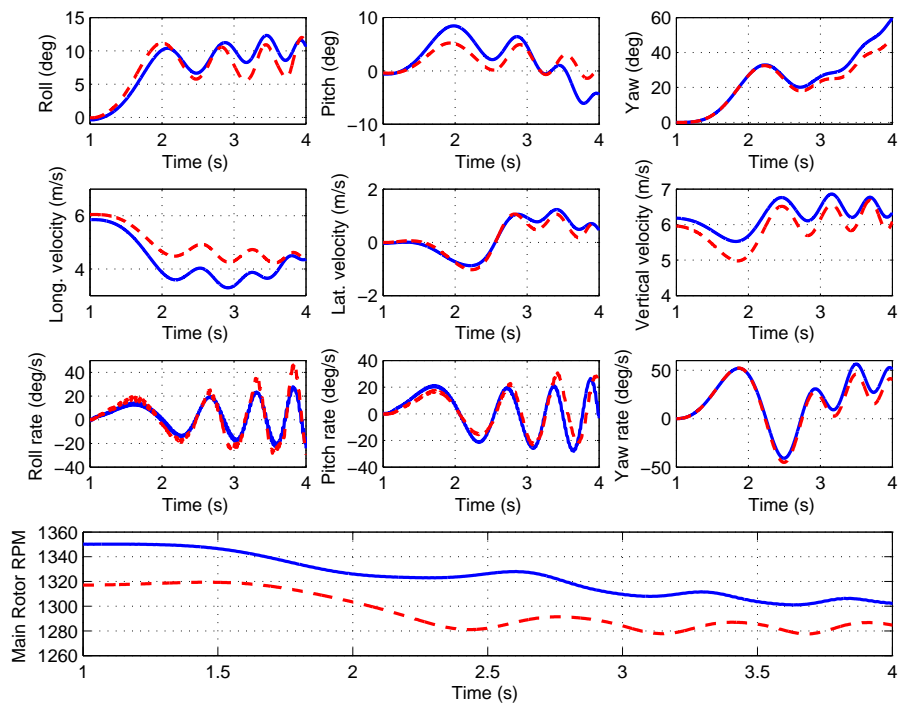


Fig. 15: Vehicle dynamics (test case 3): response to sine-sweep inputs from autorotation starting at $(V_N, V_Z) = (6, -6) \text{ m/s}$ (-FLIGHTLAB, --Our Model)

References

- [1] Boiffier, J. L., 1998. *The Dynamics of Flight The Equations*. John Wiley & Sons, Chichester, England.
- [2] Kendoul, F., 2012. "A survey of advances in guidance, navigation and control of unmanned rotorcraft systems". *J. of Field Robotics*, **29**(2), pp. 315–378.
- [3] Cai, G., Dias, J., and Seneviratne, L., 2014. "A survey of small-scale unmanned aerial vehicles: Recent advances and future development trends". *Unmanned Systems*, **2**(2).
- [4] Weilenmann, M. F., and Geering, H. P., 1994. "Test bench for rotorcraft hover control". *AIAA J. of Guidance, Control, and Dynamics*, **17**(4), pp. 729–736.
- [5] Bendotti, P., and Morris, J. C., 1995. "Robust hover control for a model helicopter". In Am. Control Conf.
- [6] Conway, A., 1995. "Autonomous control of an unstable helicopter using carrier phase gps only". PhD thesis, Stanford University.
- [7] Johnson, E. N., and DeBitetto, P. A., 1997. "Modeling and simulation for small autonomous helicopter development". In AIAA Modeling and Simulation Technologies Conf.
- [8] Grady, N. B., Frye, M. T., and Qian, C., 2006. "The instrumentation and flight testing of a rotorcraft vehicle for undergraduate flight control research". In AIAA Modeling and Simulation Technologies Conf. and Exhibit.
- [9] Cai, G., Chen, B. M., Peng, K., Dong, M., and Lee, T. H., 2006. "Modeling and control system design for a uav helicopter". In Mediterranean Conf. on Control and Automation.
- [10] Velez, C. M., Agudelo, A., and Alvarez, J., 2006. "Modeling, simulation and rapid prototyping of an unmanned mini-helicopter". In AIAA Modeling and Simulation Technologies Conf. and Exhibit.
- [11] Zhao, L., and Murthy, V. R., 2009. "Optimal controller for an autonomous helicopter in hovering and forward flight". In 47th AIAA Aerospace Sciences Meeting.
- [12] Khaligh, S. P., Fahimi, F., and Saffarian, M., 2009. "Comprehensive aerodynamic modeling of a small autonomous helicopter rotor at all flight regimes". In AIAA Modeling and Simulation Technologies Conf.
- [13] Kim, S. K., and Tilbury, T. M., 1998. "Mathematical modeling and experimental identification of a model helicopter". In AIAA Modeling and Simulation Technologies Conf.
- [14] Munzinger, C., 1998. Development of a real-time flight simulator for an experimental model helicopter. Tech. rep., Master Thesis, Georgia Institute of Technology.
- [15] Shim, D. H., 2000. "Hierarchical control system synthesis for rotorcraft-based unmanned aerial vehicles". PhD thesis, University of California at Berkeley.
- [16] Civita, M. L., 2002. "Integrated modeling and robust control for full-envelope flight of robotic helicopters". PhD thesis, Carnegie Mellon University.
- [17] Cunha, R., and Silvestre, C., 2003. "Dynamic modeling and stability analysis of model-scale helicopters with bell-hiller stabilizing bar". In AIAA Guidance, Navigation, and Control Conf.
- [18] Tanner, O., 2003. "Modeling, identification, and control of autonomous helicopters". PhD thesis, ETH Zurich.
- [19] Sudiyanto, T., Budiyo, A., and Sutarto, H. Y., 2005. "Hardware in-the-loop simulation for control system designs of model helicopter". In Aerospace Indonesia Meeting, Bandung.
- [20] Hald, U. B., Hesselbaek, M. V., and Siegmund, M., 2006. Nonlinear modeling and optimal control of a miniature autonomous helicopter. Tech. rep., Master Thesis, Aalborg University.
- [21] Bhandari, S., and Colgren, R., 2006. "6-dof dynamic model for a raptor 50 uav helicopter including stabilizer bar dynamics". In AIAA Modeling and Simulation Technologies Conf.
- [22] Cai, G., Chen, B. M., Lee, T. H., and Lum, K. Y., 2012. "Comprehensive nonlinear modeling of a miniature unmanned helicopter". *J. of the Am. Helicopter Soc.*, **57**.
- [23] Andersen, T. L., Lauritzen, D. F., Madsen, J. T., Sorensen, M. M., and Mertz, B. A., 2008. Autonomous inverted hover of a small scale helicopter. Tech. rep., Aalborg University.
- [24] Bagnell, J., and Schneider, J., 2001. "Autonomous helicopter control using reinforcement learning policy search methods". In Int. Conf. on Robotics and Automation.
- [25] Buskey, G., Roberts, O., Corke, P., Ridley, P., and Wyeth, G., 2003. *Sensing and Control for a Small-Size Helicopter. in Experimental Robotics VIII*, pp. 476-486. Springer, Berlin/Heidelberg.
- [26] Ng, A. Y., Kim, H. J., Jordan, M., and Sastry, S., 2004. "Autonomous helicopter flight via reinforcement learning". In Neural Information Processing Systems (NIPS).
- [27] Engel, J. M., 2005. Reinforcement learning applied to uav helicopter control. Tech. rep., Master Thesis, Delft University of Technology.
- [28] Amidi, O., 1996. "An autonomous vision-guided helicopter". PhD thesis, Carnegie Mellon University.
- [29] Shakernia, O., Sharp, C. S., Vidal, R., Shim, D. H., Ma, Y., and Sastry, S., 2002. "Multiple view motion estimation and control for landing an unmanned aerial vehicle". In Int. Conf. on Robotics and Automation.
- [30] Roberts, J. M., Corke, P. I., and Buskey, G., 2002. "Low-cost flight control system for a small autonomous helicopter". In Australian Conf. on Robotics and Automation.
- [31] Saripalli, S., Montgomery, J. F., and Sukhatme, G. S., 2003. "Visually-guided landing of an autonomous aerial

- vehicle". *IEEE Trans. on Robotics & Automation*, **19**(3), pp. 371–381.
- [32] Barabanov, A. E., Vazhinsky, N. Y., and Romaev, D. V., 2007. "Full autopilot for small electrical helicopter". In Europ. Rotorcraft Forum.
- [33] Gavrillets, V., Mettler, B., and Feron, E., 2001. "Nonlinear model for a small-size acrobatic helicopter". In AIAA Guidance, Navigation and Control Conf.
- [34] Mettler, B., 2003. *Identification Modelling and Characteristics of Miniature Rotorcraft*. Kluwer Academic Publishers, Norwell Mass, USA.
- [35] Marconi, L., and R.Naldi, 2006. "Robust nonlinear control for a miniature helicopter for aerobatic maneuvers". In Europ. Rotorcraft Forum.
- [36] Ng, A. Y., Coates, A., Diel, M., Ganapathi, V., Schulte, J., Tse, B., Berger, E., and Liang, E., 2004. "Autonomous inverted helicopter flight via reinforcement learning". In Int. Symposium on Experimental Robotics.
- [37] Abbeel, P., Coates, A., Quigley, M., and Ng, A. Y., 2007. "An application of reinforcement learning to aerobatic helicopter flight". In NIPS 19.
- [38] Abbeel, P., Coates, A., Hunter, T., and Ng, A. Y., 2008. "Autonomous autorotation of an rc helicopter". In 11th Int. Symposium on Experimental Robotics (ISER).
- [39] Taamallah, S., 2010. "A qualitative introduction to the vortex-ring-state, autorotation, and optimal autorotation". In Europ. Rotorcraft Forum.
- [40] Santamara, D., Viguria, A., Bejar, M., Kondak, K., and Ollero, A., 2013. "Towards autonomous autorotation landing for small size unmanned helicopters". *J. Intell. Robot Syst.*, **69**(1-4), pp. 171–180.
- [41] Taamallah, S., 2011. "Small-scale helicopter blade flap-lag equations of motion for a flybarless pitch-lag-flap main rotor". In AIAA Modeling and Simulation Technologies Conf.
- [42] Taamallah, S., 2011. "Flight dynamics modeling for a small-scale flybarless helicopter uav". In AIAA Atmospheric Flight Mechanics Conf.
- [43] Taamallah, S., 2012. "Optimal autorotation with obstacle avoidance for a small-scale flybarless helicopter uav". In AIAA Guidance, Navigation and Control Conf.
- [44] Taamallah, S., Bombois, X., and Van den Hof, P. M. J., 2012. "Optimal control for power-off landing of a small-scale helicopter a pseudospectral approach". In Am. Control Conf.
- [45] Taamallah, S., 2013. "Flatness based trajectory generation for a helicopter uav". In AIAA Guidance, Navigation and Control Conf.
- [46] Taamallah, S., 2015. "Small-scale helicopter automatic autorotation: Modeling, guidance, and control (submitted)". PhD thesis, Delft University of Technology.
- [47] Blake, B. B., and Lunn, K., 1980. "Helicopter stability and control test methodology". In AIAA Atmospheric Flight Mechanics Conf.
- [48] Tischler, M. B., and Remple, R., 2006. *Aircraft and Rotorcraft System Identification*. Am. Institute of Aeronautics & Astronautics (AIAA), Reston VA.
- [49] Padfield, G. D., 1996. *Helicopter Flight Dynamics*. Blackwell Science Ltd, Oxford, UK.
- [50] Brackbill, C. R., 2000. "Helicopter rotor aeroelastic analysis using a refined elastomeric damper model". PhD thesis, Pennsylvania State University.
- [51] Seckel, E., and Curtiss, H. C., 1962. Aerodynamic characteristics of helicopter rotors. Tech. Rep. No. 659, Department of Aerospace and Mechanical Engineering, Princeton University.
- [52] Chen, R. T. N., 1979. A simplified rotor system mathematical model for piloted flight dynamics simulation. Tech. Rep. NTM 78575, NASA Ames Research Center.
- [53] Chen, R. T. N., 1980. Effects of primary rotor parameters on flapping dynamics. Tech. Rep. NTP 1431, NASA Ames Research Center.
- [54] Gessow, A., and Myers, G. C., 1999. *Aerodynamics of the Helicopter*. College Park Pr.
- [55] Shevell, R. S., 1989. *Fundamentals of Flight*. Prentice Hall, Upper Saddle River NJ.
- [56] Anderson, J. D., 2001. *Fundamentals of Aerodynamics. Third Ed.* McGraw-Hill Higher Education, NY.
- [57] Prouty, R. W., 1995. *Helicopter Performance, Stability, and Control*. Krieger Publishing Company, Malabar, Florida USA.
- [58] Chen, R. T. N., Lebacqz, J. V., Aiken, E. W., and Tischler, M. B., 1988. Helicopter mathematical models and control law development for handling qualities research. Tech. Rep. NCR 2495, NASA Ames Research Center.
- [59] Chen, R. T. N., 1987. Flap-lag equations of motion of rigid, articulated rotor blades with three hinge sequences. Tech. Rep. NTM 100023, NASA Ames Research Center.
- [60] Ellis, C. W., 1953. "Effects of rotor dynamics on helicopter automatic control system requirements". *Aeronautical Engineering Review*.
- [61] Miller, D. G., and White, F., 1987. "A treatment of the impact of rotor-fuselage coupling on helicopter handling qualities". In Am. Helicopter Soc.
- [62] Curtiss, H. C., 1986. "Stability and control modeling". In Europ. Rotorcraft Forum.

- [63] Tischler, M. B., 1991. "System identification requirements for high bandwidth rotorcraft flight control system design". In AGARD LS-178 Rotorcraft System Identification.
- [64] Wells, D. A., 1967. *Lagrangian Dynamics*. McCraw-Hill Co.
- [65] Taamallah, S., 2011. A flight dynamics helicopter uav model for a single pitch-lag-flap main rotor: Modeling & simulations. Tech. Rep. NLR-TP-2010-286-PT-1, NLR.
- [66] Johnson, W., 1994. *Helicopter Theory*. Dover Publications Inc., NY, USA.
- [67] ART, 2006. *FLIGHTLAB Theory Manual (Vol. One & Two)*. Advanced Rotorcraft Technology, Inc., Mountain View CA.
- [68] Leishman, G. J., 2000. *Principles of Helicopter Aerodynamics*. Cambridge University Press, Cambridge, UK.
- [69] Chen, R. T. N., and Hindson, W. S., 1986. "Influence of high-order dynamics on helicopter flight control system bandwidth". *AIAA J. of Guidance, Control, and Dynamics*, **9**(2), pp. 190–197.
- [70] Takahashi, M. D., 1990. A flight-dynamic helicopter mathematical model with a single flap-lag-torsion main rotor. Tech. Rep. TM 102267, NASA Ames Research Center.
- [71] Kahaner, D., Moler, C., and Nash, S., 1989. *Numerical Methods and Software*. Prentice-Hall, NJ, USA.
- [72] Stoer, J., and Bulirsch, R., 2002. *Introduction to Numerical Analysis*. Springer-Verlag.
- [73] Chen, R. T. N., 1989. A survey of nonuniform inflow models for rotorcraft flight dynamics and control applications. Tech. Rep. NTM 102219, NASA Ames Research Center.
- [74] Kothmann, B. D., Lu, Y., DeBrun, E., and Horn, J., 2004. "Perspectives on rotorcraft aerodynamic modeling for flight dynamics applications". In 4th Decennial Specialists Conf. on Aeromechanics.
- [75] Kunz, D. L., 2005. "Comprehensive rotorcraft analysis: Past, present, and future". In AIAA/ASME/ASCE/AHS/ASC Structures, Structural Dynamics & Materials Conf.
- [76] van Hoydonck, W. R. M., Haverdings, H., and Pavel, M. D., 2009. "A review of rotorcraft wake modeling methods for flight dynamics applications". In Europ. Rotorcraft Forum.
- [77] Pitt, D. M., and Peters, D. A., 1980. "Theoretical prediction of dynamic-inflow derivatives". In Europ. Rotorcraft Forum.
- [78] Gaonkar, G. H., and Peters, D. A., 1986. "Effectiveness of current dynamic-inflow models in hover and forward flight". *J. of the Am. Helicopter Soc.*, **31**(2).
- [79] Peters, D. A., and HaQuang, N., 1988. "Technical notes - dynamic inflow for practical applications". *J. of the Am. Helicopter Soc.*, pp. 64–68.
- [80] Gaonkar, G. H., and Peters, D. A., 1988. "Review of dynamic inflow modeling for rotorcraft flight dynamics". *Vertica*, pp. 213–242.
- [81] Peters, D. A., Boyd, D. D., and He, C. J., 1989. "Finite-state induced-flow model for rotors in hover and forward flight". *J. of the Am. Helicopter Soc.*, pp. 5–17.
- [82] Peters, D. A., and He, C. J., 1991. "Correlation of measured induced velocities with a finite-state wake model". *J. of the Am. Helicopter Soc.*, **36**(3).
- [83] Peters, D. A., and He, C. J., 1995. "Finite state induced flow models part ii: Three-dimensional rotor disk". *AIAA J. of Aircraft*, **32**(2), pp. 323–333.
- [84] Hamers, M., and Basset, P. M., 2000. "Application of the finite state unsteady wake model in helicopter flight dynamic simulation". In Europ. Rotorcraft Forum.
- [85] Peters, D. A., and He, C., 2006. "Technical note: Modification of mass-flow parameter to allow smooth transition between helicopter and windmill states". *J. of the Am. Helicopter Soc.*, pp. 275–278.
- [86] Jimenez, J., Desopper, A., Taghizad, A., and Binet, L., 2001. "Induced velocity model in steep descent and vortex ring state prediction". In Europ. Rotorcraft Forum.
- [87] Keller, J. D., 1996. "An investigation of helicopter dynamic coupling using an analytical model". *J. of the Am. Helicopter Soc.*, **41**(4), p. 322330.
- [88] Curtiss, H. C., 1999. "Aerodynamic models and the off-axis response". In Am. Helicopter Soc.
- [89] Arnold, U. T. P., Keller, J. D., Curtiss, H. C., and Reichert, G., 1998. "The effect of inflow models on the predicted response of helicopters". *J. of the Am. Helicopter Soc.*, pp. 25–36.
- [90] Hamers, M., and von Grunhagen, W., 1997. "Nonlinear helicopter model validation applied to realtime simulations". In Am. Helicopter Soc.
- [91] Benoit, B., Dequin, A. M., Kampa, K., von Grunhagen, W., Basset, P. M., and Gimonet, B., 2000. "Host a general helicopter simulation tool for germany and france". In Am. Helicopter Soc.
- [92] Pitt, D. M., and Peters, D. A., 1981. "Theoretical prediction of dynamic-inflow derivatives". *Vertica*, **5**, pp. 21–34.
- [93] Bailey, F. J., 1941. A simplified theoretical method of determining the characteristics of a lifting rotor in forward flight. Tech. Rep. RNo. 716, NACA.
- [94] Houck, J. A., Moore, F. L., Howlett, J. J., Pollock, K. S., and Browne, M. M., 1977. Rotor systems research aircraft simulation mathematical model. Tech. Rep. NTM 78629, NASA Langley Research Center.
- [95] Voorsluijs, G. M., 2002. A modular generic helicopter model. Tech. rep., Master Thesis, Delft University of Technol-

ogy.

- [96] Fletcher, T. M., and Brown, R. E., 2006. “Main rotor - tail rotor wake interaction and its implications for helicopter directional control”. In *Europ. Rotorcraft Forum*.
- [97] Fletcher, T. M., and Brown, R. E., 2008. “Main rotor - tail rotor interaction and its implications for helicopter directional control”. *J. of the Am. Helicopter Soc.*, **53**(2), pp. 125–138.
- [98] Pavel, M. D., 2001. “On the necessary degrees of freedom for helicopter and wind turbine low-frequency mode-modelling”. PhD thesis, Delft University of Technology.
- [99] Talbot, P. D., Tinling, B. E., Decker, W. A., and Chen, R. T. N., 1982. A mathematical model of a single main rotor helicopter for piloted simulation. Tech. Rep. NTM 84281, NASA Ames Research Center.
- [100] Jewel, J. W., and Heyson, H. H., 1959. Charts of induced velocities near a lifting rotor. Tech. Rep. 4-15-59LY, NASA.
- [101] Baskin, V. E., Vildgrube, L. S., Vozhdayev, Y. S., and Maykapar, C. I., 1976. Theory of the lifting airscrew. Tech. Rep. TT-F-823, NASA.
- [102] Zhao, X., and Curtiss, H. C., 1988. A study of helicopter stability and control including blade dynamics. Tech. Rep. TR 1823T, NASA Ames Research Center.
- [103] ART. <http://www.flightlab.com/>, Mountain View CA., U.S.A.
- [104] Peters, D. A., Chouchane, M., and Fulton, M., 1990. “Helicopter trim with flap-lag-torsion and stall by an optimized controller”. *AIAA J. of Guidance*, **13**(5).
- [105] Peters, D. A., and Barwey, D., 1996. “A general theory of rotorcraft trim”. *Mathematical Problems in Engineering*, **2**(1), pp. 1–34.
- [106] Achar, N. S., and Gaonkar, G. H., 1993. “Helicopter trim analysis by shooting and finite element methods with optimally damped newton iterations”. *AIAA J.*, **31**(2).
- [107] Van den Hof, P. M. J., and Schrama, R. J. P., 1995. “Identification and control - closed-loop issues”. *Automatica*, **31**(12), pp. 1751–1770.

This page is intentionally left blank.

NLR

Anthony Fokkerweg 2

1059 CM Amsterdam

p) +31 88 511 3113 f) +31 88 511 3210

e) info@nlr.nl i) www.nlr.nl